GEORG-AUGUST-UNIVERSITÄT
GÖTTINGEN

Fakultät für
Physik

Bachelor's Thesis

Thrombus-Bildung an Wand-Unregelmäßigkeiten: Ein minimales Modell mit chaotischer Advektion

Thrombus Formation near Wall Irregularities: A Minimal Chaotic-Advection Model

prepared at the Max-Planck-Institute for Dynamics and Self-Organisation
by Mitja Kleider from Hannover

Thesis period: 8th March 2010 until 14th June 2010

First referee: Prof. Dr. Jürgen Vollmer

Second referee: Prof. Dr. Eberhard Bodenschatz

Contents

1 Introduction

In the present study we address general features of the interplay of the chaotic particle motion produced by hydrodynamics and active processes occuring in the blood. We focus in particular on the problem of thrombus formation.

A thrombus or blood clot is the final product of blood coagulation. Coagulation is an important part of hemostasis, which refers to the complex process of keeping blood within a damaged blood vessel.

The thrombus is a plug formed at the site of the vessel injury, its main role is the maintenance of the blood vessel integrity and the rapid cessation of bleeding. Figure 1.1 shows the formation of a blood clot, the details will be discussed further in later parts of this work.

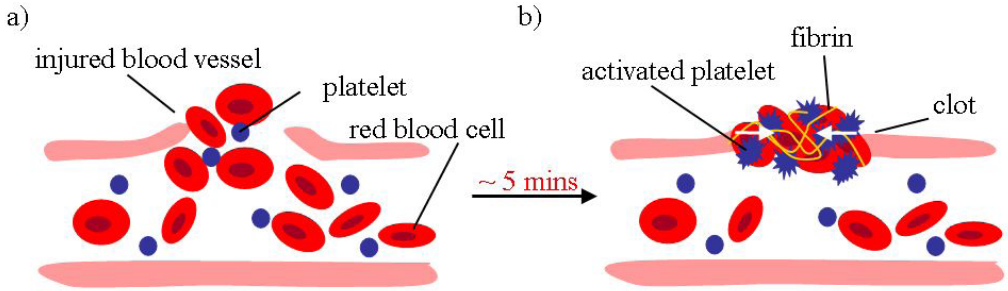

Figure 1.1: a) Quiescent platelets in the blood stream b) are activated and form a blood clot. Images by Sarah Köster.

While rapid thrombus formation is vital for survival in the event of a vascular injury, it is pathological in instances of atherosclerosis. Atherosclerosis refers to a hardening of the artery walls as a result of build-up of fatty materials. The formation of this so-called atherosclerotic plaque is based on the same processes as the thrombus formation involved in hemostasis. The plaques can gradually narrow the arteries, decreasing blood flow and resulting in pain or limited function as in angina, congestive heart failure or peripheral vascular disease. Of greater clinical

importance, plaques can also suddenly rupture, resulting in vessel occlusion that leads to death of the tissues fed by the artery in approximately 5 minutes. These events often manifest in form of a heart attack (occlusion of a coronary artery) or stroke (occlusion of a brain artery), which together are responsible for approximately half of the mortality in developed nations [2, 16].

The vascular physiology in adults is controlled by shear and pressure of the blood flow. Atherosclerosis, for instance, occurs mainly in regions of arteries that experience *disturbances* of fluid flow, namely in places where the arteries branch or turn sharply. In straight regions of the arteries, the rate of blood flow changes during the cardiac cycle, but flow is always in the same direction, and the patterns are laminar. In regions where arteries divide or curve sharply, complex flow patterns develop and the flow can reverse direction during the cardiac cycle – this is a so-called oscillatory flow. These sites show a low level of chronic inflammation, even in healthy individuals and newborn babies, that can progress to atherosclerotic plaques in older humans, if additional risk factors, such as diabetes, obesity, lack of exercise, smoking, are present [11].

Even though the risk factors play important roles in the incidence and progression of atherosclerosis, they are relatively uniform throughout the vasculature, whereas atherosclerosis is initially highly focal and occurs mainly in regions that exhibit nontrivial flow patterns. Therefore, it is the chronic exposure to disturbed flow that leads to vessel dysfunction and disease.

The aim of the present work is to investigate from a hydrodynamical point of view, how the disturbances of the flow can influence the formation of plaques and thrombi. Of particular importance are the regions of the arteries where the blood flow exhibits *chaotic motion*. Chaotic motion can occur in points where the vessel has a localized anomaly in its diameter. This anomaly can be either a constriction (stenosis, a partial blocking of the vessel), or a sudden enlargement (aneurysm). At these sites, the chaotic advection can have far-reaching consequences on the biological dynamics, a fact which was not taken into account in the traditional study of physiological and biochemical phenomena taking place in blood [27].

One of the most striking consequences of the underlying chaos is that the spatial distribution of the advected particles (chemical substances, cell fragments) is neither uniform nor smooth, and it is not stationary in time. Chaotic advection leads to a pattern formation of a new type: the particles are distributed around a filamentary fractal – like the streched thin filaments of cream in a cup of stirred coffee –,

which moves in a rhythm corresponding to the time dependence of the flow [34]. Subsequently, the chemical and biological reactions take place along this complex geometrical structure, whose characteristics can strongly influence the productivity of the reaction [33].

Examples of reactions that take place on a fractal support can be found in many natural and industrial applications, ranging from atmospheric chemistry to plankton population dynamics in oceans, and from chemical engineering to microfluidics. Some fractal images of advected particles as they appear in experiments or nature are shown in Fig. 1.2.

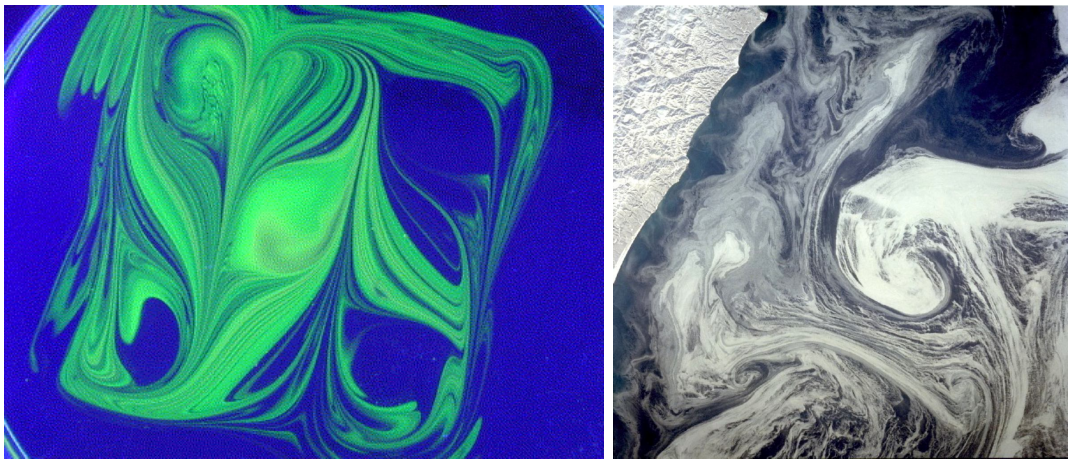

Figure 1.2: Examples of fractal structures in experiments and nature. The left image shows the shape of a dye droplet (of initial diameter about $1\,cm$) after stirring. A number of parallel cuts is made by a rod through the fluid in two directions in an alternating manner. [33] The right image shows sea-ice distribution close to Kamchatka (photograph by NASA).

In general, the fractal skeleton acts as a catalyst on the reactions, resulting in a singular enhancement of the chemical or biological activity. This enhancement was pointed out to have crucial effects on phenomena like ozone-depletion, the greenhouse effect or biodiversity [31], just to mention a few examples of major importance. A similar enhancement of the biological activity in the context of thrombus formation and progression of atherosclerosis can lead to fatalities, thus it is important to study the influence of chaotic motion. For this purpose we construct a minimal chaotic advection model that also incorporates the biological reactions involved in thrombus formation, and we identify the basic factors influencing the productivity of the reactions.

2 Basic concepts

2.1 The advection problem

The transport of a substance or a scalar quantity (such as concentration or temperature) by a fluid flow with a velocity field $u(\vec{r}, t)$ is called advection. The theory of dynamical systems provides the proper tools for the description of advection dynamics [21, 30]. In the advection problem advected particles are called *tracers*. Pointlike, massless tracers, that take on the velocity of the flow immediately, are called *passive tracers*. Particles that participate in chemical or biological reactions, or influence the flow field, are considered *active tracers*. A scalar quantity advected by a flow is usually referred to as *passive scalar*.

Its motion from an initial position $\vec{r}(t)$ is described by a set of ordinary differential equations

$$\frac{\mathrm{d}\vec{r}(t)}{\mathrm{d}t} = \vec{u}(\vec{r}, t). \tag{2.1}$$

An appealing property of hydrodynamical systems [35] is that the phase space of the particle dynamics coincides with the configuration space and thus the phase space structures are directly observable.

2.2 Chaotic advection

Even in simple two-dimensional, time periodic flows the advection dynamics can be very complex and is often chaotic [6].

Chaotic motion appears due to the presence of hyperbolic fixed points in phase space [22]. Fixed points appear in *stroboscopic maps* of the flow, which are series of snapshots taken at integer multiples of the period of the flow. In this map fixed points represent periodic orbits, i.e., closed particle trajectories along which the motion is repeated periodically in time. Due to the incompressibility of the flow fixed points can be stable (elliptic) or unstable (hyperbolic) [30]. If the fixed point

is *hyperbolic* or unstable, a small perturbation moves off particles from it. If the fixed point is *elliptic*, perturbations lead to trajectories that remain close to it.

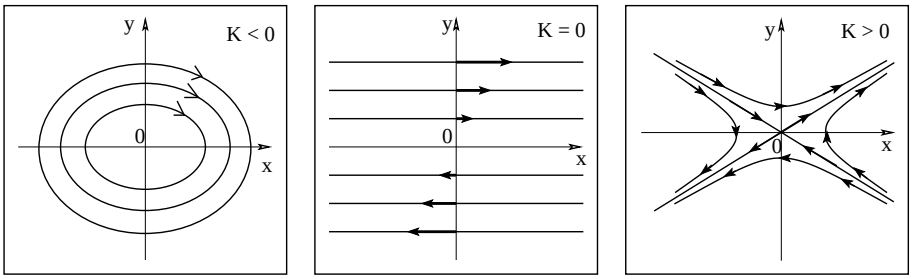

Figure 2.1: Trajectories in a flow field given by $u_x = Gy$, $u_y = GKx$, with the constants $G, K \in \mathbb{R}$ [22]. Elliptic fixed point (left panel), hyperbolic fixed point (right panel).

Hyperbolic points have saddle point structure: we can associate a stable and unstable direction to each of them (see the right panel of Fig. 2.1). The stable direction points towards the fixed point, the unstable direction points away from the fixed point. Particles situated close to the stable direction can approach the fixed point for possibly a very long time. However, eventually they also leave the vicinity of the fixed point along the unstable direction (see the outer arrows in Fig. 2.1).

The chaotic motion is caused by a set of unstable fixed points [3] that form the so-called *chaotic set* or *chaotic saddle*. The unstable directions of these individual points form the unstable manifold, the stable directions form the stable manifold. Manifolds of the same type cannot have intersections and self-intersections, but stable and unstable manifolds belonging to the same point or to different points intersect each other in infinitely many points [1, 8]. These intersections are responsible for the complex behavior of chaotic flows [7].

The elliptic points can appear only in conservative systems. When they are present, they are sourrounded by regular orbits (see the ellipses in the left panel of Fig. 2.1). In a two-dimensional phase space these regular orbits act as transport barriers separating different chaotic regions. They form the so-called Kolmogorov-Arnold-Moser (KAM) tori [21].

2.3 Open chaotic flows

Open flows are characterized by unbounded particle trajectories. We consider flows that are stationary everywhere but in the mixing region. A particle's motion is simple in the inflow and outflow regions, but typically chaotic in the mixing region, i.e., typical trajectories experience chaotic behavior only for a finite time while they reside in a finite region in space. Consequently, chaos is of *transient* type [29]. Transiently chaotic systems are characterized by their *non-escaping orbits*. These orbits are the unstable fixed points of the stroboscopic map. They form a fractal set, which is called the *chaotic saddle* or *chaotic set*. The saddle can be reached from a set of exceptional initial positions. The union of all initial positions that converge to non-escaping trajectories is the *stable manifold* of the chaotic saddle [23]. Particles starting far away from the stable manifold are leaving the mixing region quickly, but tracers starting close to the stable manifold are advected towards the chaotic saddle. They follow a non-escaping orbit for a while, then they are trapped by the stable manifold of another non-escaping orbit and so on, until they leave the chaotic saddle along its *unstable manifold* [23].

The unstable manifold can be visualized by a droplet of dye placed into the flow: the dye particles trace out the permanent fractal pattern of the unstable manifold [32]. The stable manifold of the conservative flow can also easily be found since it is the image of the unstable manifold with regard to time reversal symmetry [18, 25].

2.4 Closed chaotic flows

Closed flows are characterized by tracer trajectories confined to a bounded region. The chaotic motion is due to a set of hyperbolic fixed points also in this case. In contrast to the open case where the stable and unstable manifolds had fractal structure, the stable and unstable foliations of closed flows are two-dimensional objects. After all, chaotic systems are mixing, and according to ergodic theory any initial tracer distribution weakly approaches the uniform distribution in a mixing conservative flow.

Accordingly, a droplet of dye will move along the unstable foliation and visualize some part of it for a while (Fig. 2.2). For larger times the dye will be uniformly distributed in the two-dimensional plane of the flow [22, 30].

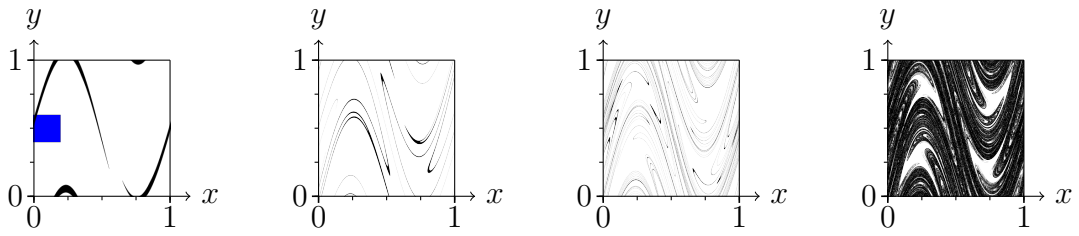

Figure 2.2: Shape of a square droplet (blue) at times $t/T = 1, 2, 3$ and 6, advected by an alternating sinusoidal shear flow (see Section 4.2).

The main differences between open and closed chaotic flows can be summarized in the following scheme:

	type of chaos	**fractal structures**
open flow	transient	permanent
closed flow	permanent	transient

2.5 Quantifying chaotic motion

The chaotic dynamics is characterized by unpredictable motion in the long term, and by the appearance of complex, yet ordered geometrical structures in the phase space [4, 5, 21, 30].

The unpredictability of chaotic motion is due to the sensitivity of chaos to initial conditions: two initially infinitesimally close trajectories will deviate exponentially in time.

- The **Lyapunov exponent** λ is the measure of unpredictablility, that characterizes the divergence of the initially close trajectories [21, 30]:

$$\delta\vec{r}(t) = \delta\vec{r}(0) \cdot e^{\lambda t} \quad \text{or} \quad \lambda = \lim_{t\to\infty} \lim_{\delta\vec{r}\to 0} \frac{1}{t} \ln \frac{|\delta\vec{r}(t)|}{|\delta\vec{r}(0)|}, \tag{2.2}$$

  where $\delta\vec{r}(t)$ represents a vector (much smaller than the system size) connecting two trajectories belonging to different initial conditions after time t. The Lyapunov exponent is determined from the scaling regime of a $\ln(\delta\vec{r})$ vs t plot.

A negative Lyapunov exponent λ' can also be defined characterizing the exponential contraction along the stable manifold. A phase space volume element (a droplet) is

stretched by a factor $e^{\lambda t}$ along the unstable manifold, and contracted by a factor of $e^{\lambda' t}$ along the stable manifold.

The chaotic dynamics is associated with the appearance of complex geometrical objects in phase space. These objects, like the chaotic saddle or its unstable manifold, are sets of measure zero and have a well defined, ordered, and fractal structure. They can be characterized by the following quantities:

- The **fractal dimension** D is a statistical quantity indicating how completely space is filled by a fractal. The *box-counting dimension* is defined [21, 30] by

$$\mathcal{N}(\varepsilon) \propto \varepsilon^{-D} \quad \text{or} \quad D = \lim_{\varepsilon \to 0} \frac{\ln \mathcal{N}(\varepsilon)}{\ln(1/\varepsilon)}, \tag{2.3}$$

  where ε is the linear size of the box, and $\mathcal{N}(\varepsilon)$ is the number of boxes needed to cover the fractal. In contrast to 1-dimensional lines or 2-dimensional planes, the dimension is a non-integer value: $1 < D < 2$ in case of a fractal embedded in the 2-dimensional plane.

- The **escape rate** κ is a statistical measure of openness, defined by the exponential decay of the number of tracers in the mixing region [29, 30] as:

$$N(t) = N(0)e^{-\kappa t}, \quad \text{giving} \quad \kappa = -\frac{1}{t} \ln \frac{N(t)}{N(0)}. \tag{2.4}$$

  For a closed system $\kappa = 0$, since $N(t)$ remains constant and equal to $N(0)$ for all times t.

- The **residence time** is the time a tracer spends in the mixing region. This time strongly depends on whether the tracer is close to the stable manifold or not. Since the stable manifold has a complex structure that is non-differentiable in space, accordingly, the residence time of the particles will also show strong irregularities in space. $1/\kappa$ can be considered the average lifetime of transient chaos [10] or residence time.

The **Kaplan-Yorke relation**, established for chaotic attractors, explicitly connects the fractal dimension to the Lyapunov exponents [30]. The fractal dimension of the attractor is given by

$$D = 1 - \frac{\bar{\lambda}}{|\bar{\lambda}'|}, \tag{2.5}$$

where $\bar{\lambda}$ is the average Lyapunov exponent in the expanding direction (along the unstable manifold) while $\bar{\lambda}'$ is the average Lyapunov exponent in the contracting direction (along the stable manifold).

A modified version of Eq. (2.5) was established for the case of open flows by Kantz and Grassberger [13, 15]. In this case the Lyapunov exponents are connected to the dimension of the *chaotic saddle* by the so-called Kantz-Grassberger formula:

$$D \approx 1 - \kappa/\bar{\lambda}, \tag{2.6}$$

where κ is the escape rate of the chaotic saddle.

2.6 Chemical and biological reactions in chaotic flows

In many applications species advected by a fluid flow participate in chemical reactions or biological processes at the same time. Such flows in which some kind of chemical or biological activity takes place are referred to as *reactive* or *active flows*. Reactive flows play an important role in nature and technology and they are ubiquitous in the atmosphere and the oceans.

The characteristic features of the interplay between mixing and chemical reactions depend on the type of chemical reaction dynamics considered. Below we enumerate some of the most important classes studied in the literature (see [33] and references therein):

- **Autocatalytic reactions:** $A + B \to 2B$. The dynamics of plankton blooms (nutrient + plankton $\to$ more plankton) belong to this category. The complex interactions of nutrients and plankton species in the oceans are influenced by stirring due to the mesoscale eddies. Since plankton plays a crucial role in the carbon exchange between oceans and atmosphere, this problem can influence the greenhouse effect.

- **Decaying chemical reactions.** The case of linear ($B \to 0$) and second order ($2B \to B$) decay was studied in the context of atmospheric ozone chemistry, where the interaction between transport processes and chemical reactions leads to the formation of the ozone hole in the polar regions of the stratosphere.

- **Acid-base reactions:** $A + B \to C$. In this case a source of both components is needed.

- **Competition of species** involves two species B_1 and B_2 competing for the same resource (food) A: $A + B_1 \to B_1$; $A + B_2 \to B_2$. This problem is relevant to the question of biodiversity in aquatic ecosystems.

- **Oscillating reactions** like Belousov-Zhabotinsky reactions, or metabolic cycles that involve many species.

As described in Section 2.3, the stirring process typically leads to the formation of complex filamental distributions of the advected particles: they trace out the unstable manifold of the chaotic saddle. If chemical or biological reactions are superimposed into the advection dynamics, the products of the reactions will fatten up the unstable manifold: they cover the filaments of the unstable manifold with a

finite coverage width. The structures formed in this way provide sensitive mechanisms that enhance chemical and biological activity in flows.

The many kinds of cells and organic molecules making up blood participate in a multitude of chemical reactions and biological interactions. If chaotic advection is present in the blood flow, it can have strong effects on the rates and other properties of these processes. On one hand, the distribution along filaments of the advected substances can influence the productivity of the reactions. On the other hand, chaos induces a large increase in the average residence time of the advected particles, thus they will have more time to adhere to the vessel wall.

2.7 Master equations

In cases when the advection dynamics are not chaotic, the flow can be considered well-mixed, and the spatial distribution of the advected particles is uniform [33]. In these cases a mean-field approach can be adopted. One of the most significant tools to describe the dynamics of such a system is the *master equation* [12].

The master equations are formulated in terms of probabilities of the system to be in a given state m at time t. The probability to encounter the system in the state m at time t is *increased* by transitions from other states m' to m and is *decreased* by transitions leaving the state m:

$$\dot{P}(m,t) = \text{incoming ratio} - \text{outgoing ratio}. \tag{2.7}$$

The incoming ratio consists of all transitions from any state m' to m and therefore consists of the sum over all states. Each single term is the probability P to find the system at the state m' multiplied by the probability w of a transition from m' to m:

$$\text{incoming ratio} = \sum_{m'} w(m,m')P(m',t). \tag{2.8}$$

We also used the *Markov assumption*: we assume that the transition process has no memory, which means that the transition probability to a new configuration only depends on the previous configuration, not on any configuration in further history.

With this assumption the outgoing ratio consists of all possible transitions from

the state m to any other state m':

$$\text{outgoing ratio} = P(m,t) \cdot \sum_{m'} w(m',m). \tag{2.9}$$

The resulting equation after inserting (2.8) and (2.9) into (2.7) is the so-called **master equation**:

$$\dot{P}(m,t) = \sum_{m'} w(m,m')P(m',t) - P(m,t) \cdot \sum_{m'} w(m',m). \tag{2.10}$$

In most cases the incoming and outgoing ratios can be specified easily, the determination of the transition probabilities w is usually more complicated.

Even though in many cases it may be difficult to find the exact analytical solutions of the master equations, usually the *steady state solutions* can easily be obtained from the linear equations. In the steady state the incoming and outgoing ratios are equal, this means that the probability to encounter the system in the state m does not change in time, giving the condition $\dot{P}(m,t) = 0$. We obtain the steady state solutions by solving the resulting linear equation:

$$P(m,t) = \sum_{m'} \frac{w(m,m')}{\sum_{m''} w(m'',m)} P(m',t). \tag{2.11}$$

3 Numerical methods

Several well-established numerical methods are used to visualize and characterize the states and dynamics of our model.

- **Visualization of the chaotic saddle and its stable and unstable manifold.** To obtain the chaotic invariant sets we follow the method described in [28]. We start with a large number of particles $N(t = 0)$ initially uniformly distributed in the full phase space. All non-escaping particles are followed over a large number of iterations n. For large enough $N(0)$ and n, the initial coordinates of the non-escaping particles should trace out the stable manifold, their final positions after n steps should trace out the unstable manifold, and the mid-points at time $\frac{n}{2}$ should trace out the chaotic saddle. The reason is that all initial points from the chaotic region exit with the exception of a fractal set of measure zero. Therefore, points spending a long time in the system must be those that came close to the chaotic set. The points still inside after n steps are thus either on the chaotic saddle or are already about to leave it. If so, they are practically on the unstable manifold. A long time ($\frac{n}{2}$ steps) earlier they must have been around the saddle, and initially around the stable manifold.

- **Measuring the dimension of fractal regions and boundaries.** To determine its *box-counting* dimension, a region is covered with boxes of size ε, then the number $\mathcal{N}$ of non-empty boxes is counted. These steps are repeated with different box sizes. We plot $\ln \mathcal{N}(\varepsilon)$ versus $\ln \varepsilon$ and measure the slope, which is the box-counting dimension [5, 20, 21, 30].

  To determine the dimension of a fractal boundary, only the boundaries of the region are covered with boxes. The further procedure is the same as above.

- **Measuring Lyapunov exponents.** If the flow field is given by an analytical formula, we can linearize it around a fixed point. The time evolution of the

distance Δx can be obtained by iterating the linearized equations. The logarithm of the ratio $\Delta x_i/\Delta x_{i-1}$ averaged over a long time gives a good estimate for the average Lyapunov exponent [30].

- **Measuring escape rates.** At each time step we measure the number $N(t)$ of non-escaped particles in the mixing region. We follow the dynamics until the number of particles has decreased by approximately one order of magnitude. The slope of the $\ln(N)$ versus t plot gives the escape rate [28].

4 A minimal model for thrombus formation near wall irregularities

For modeling thrombus formation near wall irregularities, we need specific information on the hydrodynamical and biochemical characteristics of the phenomenon that goes beyond the level of the basic concepts reviewed in the previous chapter. In this chapter we present first a short background on blood flow near wall irregularities (Section 4.1) in parallel with the model we use to model the flow (Section 4.2). Next, we briefly summarize the biological processes involved in thrombus formation (Section 4.3), and in parallel we present the biological model we propose to study (Section 4.4).

Regarding the hydrodynamical part, our model is based on a recent work [27] that reported chaotic advection in the presence of vessel wall irregularities. The biological part is based on recent literature [9, 11, 16] regarding the dynamics of platelets (particles involved in thrombus formation), and on communication with Thomas Pfohl at the Max-Planck-Institute for Dynamics and Self-Organization and Sarah Köster at Georg-August-Universität Göttingen.

4.1 Chaotic advection in blood flow

Blood flowing through the vasculature forms a closed system. However, from the point of view of a phenomenon that is observed in a finite part of the vascular system, the blood flow is locally open: there is a net current of blood flowing through the region of observation. Particles transported by the blood enter the region of interest, spend some time in this region, and then they usually leave downstream.

As an open flow with a time periodicity determined by the cardiac cycle, the blood flow can exhibit chaotic advection under certain circumstances. Chaotic advection was pointed out to appear in points where the vessel has a localized anomaly in its diameter [27]. This anomaly can be either a constriction (a stenosis, partial blocking

of the vessel) or a sudden enlargement (an aneurysm). In the work of Schelin et al. [27] the typical streamlines of the blood flow near these types of wall-irregularities were obtained by using the finite-volume solver *Fluent* for realistic physiological conditions (dynamic viscosity $\mu = 0.04\, g/cm \cdot s$, and density $\rho = 1.06\, g/cm^3$). Two cases were studied, namely (i) partly blocked vessels in coronary arteries (Fig. 4.1, left panels), and (ii) aneurysms in abdominal aortas in exercise conditions (right panels). The time period of the blood flow in excercise conditions is $T \approx 0.45\, s$, its typical velocity is $v = 10\, cm/s$. The obtained streamlines are shown in Fig. 4.1 for

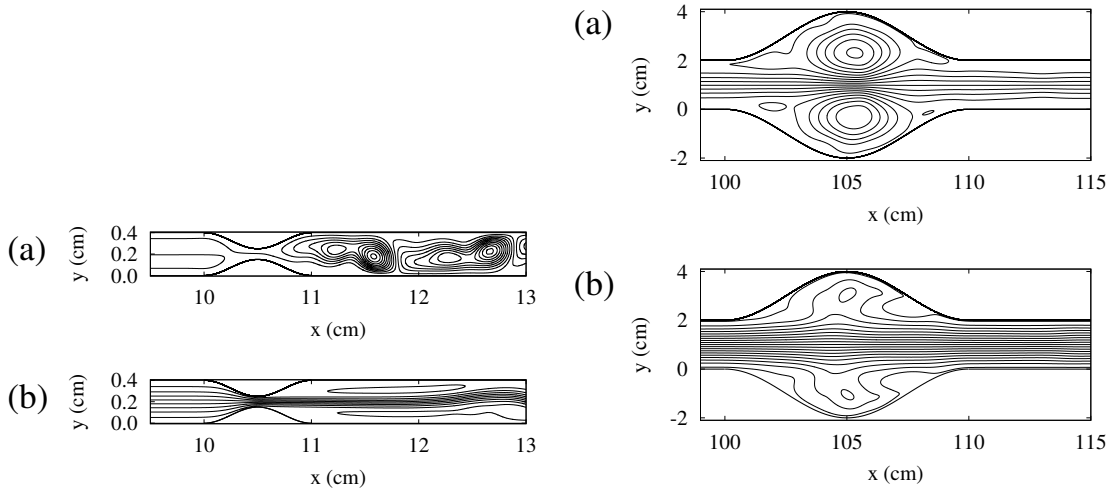

Figure 4.1: Snapshots of the streamlines of the blood flow in the 2D model of an obstructed coronary artery (left), and abdominal aorta with aneurysm (right). Time instances correspond to the minimum (a) and maximum (b) blood velocity in the cardiac cycle. [27]

two different time instances: (a) when the inlet velocity has a minimum $v_{min} = 0$ in case of the coronary artery, and $v_{min} = 20\, cm/s$ for the abdominal aorta, and (b) for maximal inlet velocities $v_{max} = 40\, cm/s$ for both the coronary artery and abdominal aorta.

Even though the blood flow field is regular and non-turbulent in the presented cases, the advection dynamics is chaotic. The advected particles are distributed in both cases along a filamentary fractal typical to chaotic advection (see Fig. 4.2). The filaments represent the unstable manifold of the chaotic saddle responsible for the chaotic motion. These fractals have a fractal dimension $D = 1.72 \pm 0.02$ in case of the coronary artery, and $D = 1.67 \pm 0.02$ for the abdominal aorta.

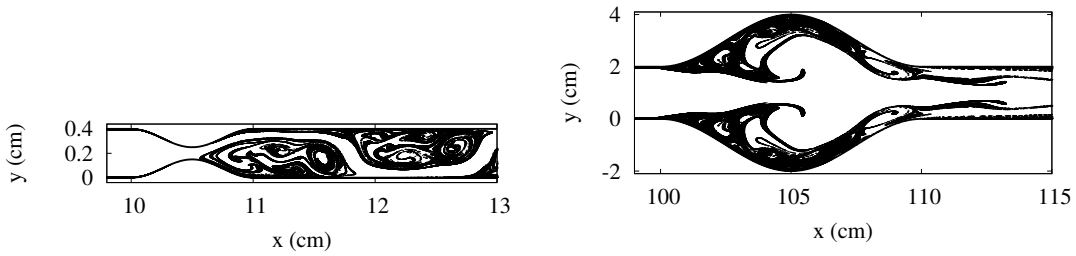

Figure 4.2: Snapshots of the unstable foliation of blood flow in the stenosed coronary artery (left) and in the aorta with aneurysm, respectively (right). [27]

A consequence of the fractal spatial distribution of the advected particles is their increased residence time in the region of observation. The average residence time was found to be $\tau = 19.2\,s$ for the coronary artery and $\tau = 2.01\,s$ for the abdominal aorta, which is considerably larger than the residence time of a particle advected by a laminar blood flow. The latter is given by the period of the cardiac cycle, that is $\tau_{laminar} = 0.45\,s$.

The chaotic trajectories were also characterised by sensitive dependence on the initial conditions that can be quantified by Lyapunov exponents. The Lyapunov exponents were found to be $\lambda = 0.187\,s^{-1}$ for the coronary artery, and $\lambda = 1.648\,s^{-1}$ for the abdominal aorta.

4.2 The chaotic flow model

As a workbench system we use a time periodic, two dimensional flow defined in the unit square with periodic boundary conditions that is known to produce chaotic trajectories [24]. The flow consists of the alternation of two steady sinusoidal shear flows in the x and y directions, respectively. Advection by this flow field over one time period is equivalent to the action of the two-dimensional, area preserving map [20, 28] defined as:

$$\begin{aligned} x_{n+1} &= x_n + a\sin(2\pi\, y_n + \varphi) \bmod 1, y_{n+1} = y_n \qquad \text{in the first } \tfrac{T}{2}, \\ y_{n+1} &= y_n + a\sin(2\pi\, x_n + \varphi) \bmod 1, x_{n+1} = x_n \qquad \text{in the second } \tfrac{T}{2}, \end{aligned} \tag{4.1}$$

where x_n and y_n denote the coordinates of a fluid particle at discrete times $t = n \cdot \frac{T}{2}, n \in \mathbb{N}$, and T is the period of the flow. The amplitude a is a parameter that controls the chaotic behavior of the flow.

One problem that generally appears in area-preserving (i.e., conservative) maps is the existence of quasiperiodic orbits that form KAM tori. These tori act as transport barriers separating different chaotic regions. The size of these KAM tori can be minimized by tuning the parameters of the map. In the map defined by Eq. (4.1) there are four regions that contain KAM tori, as depicted by the white islands in Fig. 2.2, where $a = 0.6$, $\varphi = 0$ was used. These islands exist for small amplitudes a, and they gradually disappear for higher values of a.

In numerical simulations we use the value $a = 0.6$ for the amplitude of the flow. For this value the phase space consists of one single chaotic region without visible KAM tori. The advection dynamics is still affected by remnants of the KAM tori: Particles that start outside the islands remain outside for a while, but might enter the islands after a long time. This is the reason why the white islands are still visible after a short time in Fig. 2.2. Similarly, particles starting inside the islands will visit only points in the interior of the island, before they finally escape to the larger outside region. To avoid effects from the remnants of KAM tori, we also run simulations for higher amplitudes of the flow ($a = 0.8$ and $a = 1.4$).

A more efficient way to avoid effects of the KAM tori is to consider φ as a random variable $\varphi_n \in [0, 2\pi]$ taking on different values in each step of the iteration. In this case the flow is aperiodic. An alternative approach is to keep $\varphi = 0$, but change the sign of the amplitude a randomly. This approach minimizes the effects from KAM tori as well. In Chapter 5 we investigate cases with $a = 0.6$, $a = 0.8$, and $a = 1.4$, $\varphi = 0$ (deterministic case), compared to $a = 0.6$, and random phase φ (case of aperiodic flow). In Chapter 6 we study the case of flows with randomized amplitude sign for $|a| = 0.6$, and $|a| = 6.4$, and keep a fixed phase $\varphi = 0$.

The map defined by Eq. (4.1) produces a closed flow. As the blood flow is an open flow, in numerical simulations we follow a standard "leaking" mechanism proposed by Schneider et al. in [28]: We consider a "leak" in the unit square, i.e., we define a spatial area through which particles can enter and/or escape the mixing region. More details on the effects of leaking the closed system of Eq. (4.1) can be found in Appendix B. The exact shapes and sizes of the leaks, i.e., of the inflow and outflow regions we used in this work, are defined in Sections 4.4.1 and 4.4.2. They are shown as blue and black areas for inflow and outflow, respectively, in Figs. 4.5, and 4.8.

The positions (x_n, y_n) are in $\mathbb{R}^2$. For plotting the spatial distribution at each half period, the positions are aligned[1] to a discrete, Cartesian $N \times N$ lattice of length

[1]Specifically, to map each position to the respective lattice point, the real numbers $x_n, y_n \in [0, 1)$

and height unity with spacing $\Delta x = \Delta y = \frac{1}{N}$ ($N = 1000$ in our plots).

4.3 Dynamics of thrombus formation

In case of a vascular injury, hemostasis is achieved by the activation and aggregation of platelets that form a platelet plug or thrombus at the site of the injury (Fig. 1.1).

Platelets (thrombocytes) are small, $2-3\,\mu m$ in diameter, a-nuclear cell fragments (i.e., cells that do not have a nucleus containing DNA), released from the bone marrow into the blood stream. Under normal conditions, platelets circulate freely in the blood and do not adhere to each other or to the vessel wall.

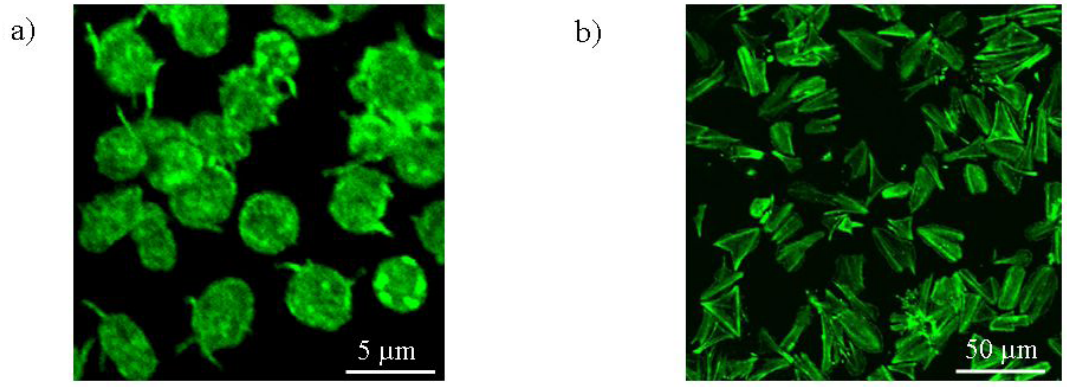

Figure 4.3: Fluorescent micrographs of a) quiescent platelets and b) activated platelets. Note that the scale bars are different. Images by Sarah Köster.

When a vascular injury occurs, the cells of the damaged vessel wall release proteins as collagen, thrombin, or the so-called *von Willebrand factor* to the blood stream. Binding of von Willebrand factor to other proteins is most efficient under high shear stress [26]. These proteins can activate the otherwise passive platelets. Activated platelets change in shape (Fig. 4.3), and pseudopods form on their surface. The activated platelets aggregate or clump together using different connecting agents, and adhere to the vessel wall. Aggregation and adhesion act together to form the platelet plug that stops the bleeding until the vessel wall is fully repaired.

The same processes are encountered in the pathogenesis of atherosclerosis, where the aggregated platelets form the atherosclerotic plaque. The activation is triggered

are multiplied by N and rounded to integer values. These integer values correspond to the indices of a lattice point.

by the same chemical factors, but the deposition occurs in places where the flow experiences disturbances.

The details of the activation process are quite complex and a topic of very active present research [9, 11, 14, 16, 17]. However, for the purposes of the present study we consider two idealized scenarios:

(A) Platelets are activated by a number of agents that are mainly secreted by the vessel wall. Thus in modeling the phenomena we assume that platelets are activated when they enter certain spatial regions that are rich in particles triggering activation (i.e., upon close approach to the damaged vessel wall). The corresponding model is described in Section 4.4.1.

(B) Platelets are activated by high shear stress in the blood flow. To incorporate this factor in our model, we identify (time-dependent) regions of high shear in the blood stream, and assume that activation occurs in these regions. This model is described in Section 4.4.2.

For the deposition of platelets we also consider two distinct cases. In the first case (A) we consider that aggregation and deposition of platelets takes place in well defined spatial regions. This is most relevant to hemostasis, where the thrombus is formed at the site of the injury. In the other case (B) we consider that deposition takes place in regions defined by low shear rates. This mimics the formation of atherosclerotic plaques. The slow flow in these regions promotes attachment, while low shear helps particles to remain bounded to the vessel wall.

4.4 Minimal models for thrombus formation

In modeling the biological dynamics, we do not keep evidence of the complex chemical reactions needed to activate passive platelets. Instead, we simply define spatial regions, where the probability of activation is high (due to wall injury, high concentration of activators, high shear, or other factors), and suppose that passive platelets are activated instantaneously upon entering these regions. We refer to these regions as *activation regions*. Similarly, we define the *deposition regions* as the areas where active platelets have a high probability to attach to the vessel wall, and assume that all active platelets visiting these regions are deposited instantaneously.

The proper tool to describe such a dynamics is the *resetting forcing* proposed by Neufeld et al. in [20]. Following this method, we consider a particle-based,

i.e., Lagrangian picture. In this view, a fluid element moves as a particle, and can have three different types: "passive" if it contains a passive platelet, "active" if it carries an active platelet, and "empty" if the platelet has been deposited from the fluid element under consideration. Particles are advected according to Eqs. (4.1) and their types are conserved along their trajectories except for the activation and deposition regions. In the activation region the type of passive platelets is changed (i.e., reset) to active, while in the deposition region the type of active platelets is reset to deposited or empty, depending on whether we talk about platelets or the fluid elements carrying them, respectively.

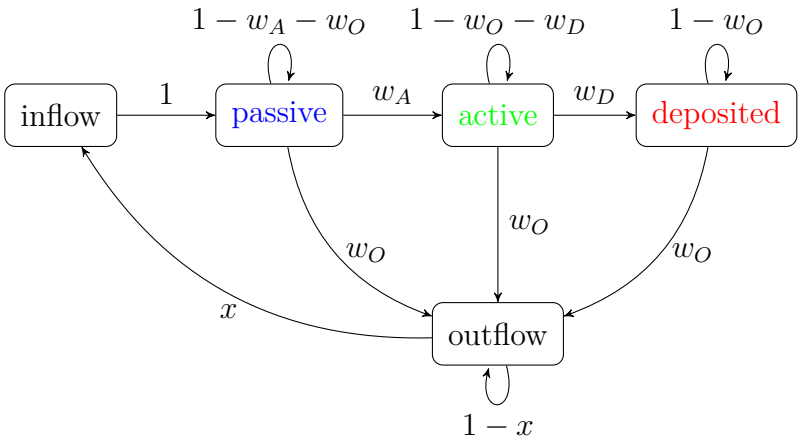

Figure 4.4: Schematic representation of the biological dynamics: Each of the transitions has a given probability depicted on the arrows. For one initial droplet $x = 0$, platelets leaving will not return. For the mean-field approximation we consider that the same amount of platelets or empty fluid elements that is leaving the system is returning as "fresh" passive platelets, thus $x = 1$.

The platelet dynamics is much more complex than the case described in [20] that considers only two types of particles. For details on resetting two types of particles see Appendix C. The main difference is the selective sensitivity of the resetting domains on the type of particles: in the activation region the passive particles are reset only, the empty particles remain unchanged. Similarly, in the deposition region only the active platelets are deposited, i.e., only that subset of particles that has visited the activation region at an earlier time. All other particles (passive or empty fluid elements) will leave the deposition region without any change in their types.

As in Section 4.3 we treat two distinct cases as follows.

4.4.1 Modelling platelet activation at the vessel wall

In this case the positions of the activation and deposition regions are constant in time and do not depend on the flow. This case represents for instance activation of the platelets at the site of a vessel injury, whose position is fixed and does not change in time. Similarly, deposition also takes place at the vessel wall where the damage occured, i.e., in a well defined spatial region that does not change in time.

We consider an inflow of fresh blood containing passive platelets to the mixing region. Since the particles engaged in chaotic motion visit all parts of the system in sufficiently long time, the exact position of the inflow region does not have significant effect on the behavior of the particles. Without loss of generality, we can therefore define the inflow region as a horizontal stripe of width w_I and length unity centered at $y = 0.5$.

The same argument is valid for the biological dynamics: the main characteristics of the reactions are not influenced by the exact position of the activation and deposition regions. Thus, for the sake of convenience (i.e., to avoid additional effects caused by overlapping areas), we consider that these regions are also stripes that are situated parallel to the inflow region. The activation region is a stripe of width w_A and length unity centered at $y = 0.75$, while the deposition region is a stripe of width w_D and length unity centered at $y = 0.25$. The stripes are shown in Figure 4.5. To keep the number of the parameters as low as possible in the model, we consider only cases where the two stripes have the same width, i.e., $w_A = w_D = w$.

In contrast to the position, the size of the activation and deposition regions is expected to have strong influence on the dynamics. Thus in the numerical simulations we keep constant the size of the inflow region w_I and change the size of the activation and deposition regions w in steps of 0.01 from $w = 0.01$ to $w = 0.3$.

4.4.2 Modelling shear-induced platelet activation

In this case, we consider activation and deposition regions that change in time according to the periodicity of the flow. This represents the case of platelets that are activated by high shear rates of the blood flow and deposited in regions of low shear, thus it is more typical to the formation of atherosclerotic plaques triggered by disturbances of the flow.

The shear rate S can be obtained as the derivative of the equations defining the

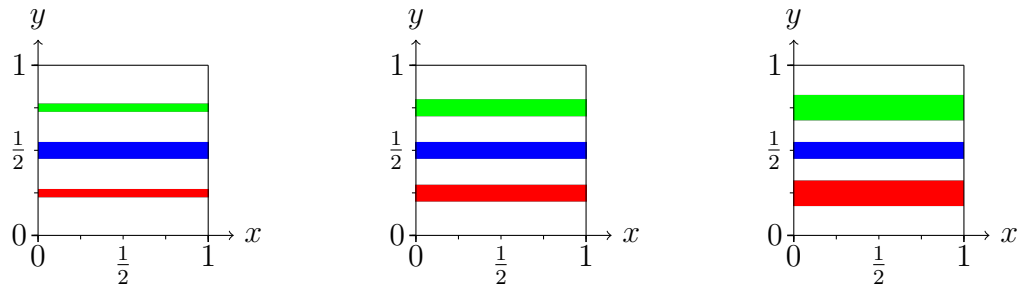

(a) $w = 0.05$ (b) $w = 0.10$ (c) $w = 0.15$

Figure 4.5: Horizontal stripes marking the regions of inflow (blue), activation (green) and deposition (red). The width of the inflow region is $w_I = 0.1$.

velocity field. In our particular flow model (Eq. (4.1)) this gives

$$\begin{aligned} S_y = \tfrac{du_y}{dx} &= |2\pi a \cos(2\pi x)|, S_x = 0 \text{ for the first } \tfrac{T}{2}, \\ S_x = \tfrac{du_x}{dy} &= |2\pi a \cos(2\pi y)|, S_y = 0 \text{ for the second } \tfrac{T}{2}. \end{aligned} \tag{4.2}$$

We define a normalized shear that takes values $0 \leq s \leq 1$:

$$s = \frac{S}{2\pi|a|}. \tag{4.3}$$

The biological dynamics for shear-induced activation and deposition are defined as follows: Platelets are activated in regions of high shear. We assume that activation of the platelets takes place in spatial regions where the shear is higher than a certain threshold. Thus we define the activation region by the condition:

$$1 \geq s > 1 - \alpha. \tag{4.4}$$

Active platelets will be deposited where the shear rate is low, i.e.,

$$0 \leq s < \beta, \tag{4.5}$$

where α and β are free parameters that can be tuned in simulations to identify their effects.

From Eq. (4.3) and the conditions (4.4) and (4.5) results that the regions of activation and deposition are horizontal stripes for half a period and vertical stripes

for the other half of the period. The width of the stripes is

$$\begin{aligned} w_A(\alpha) &= 4 \cdot \tfrac{\arccos(1-\alpha)}{2\pi}, \qquad \text{and} \\ w_D(\beta) &= 1 - 4 \cdot \tfrac{\arccos(\beta)}{2\pi}. \end{aligned} \tag{4.6}$$

In the following we treat two distinct cases: (i) the regions of activation and deposition have the same area in space ($w_A = w_D$), and (ii) the regions represent equal ranges in terms of shear ($\alpha = \beta$).

(i) In the first case the regions of activation and deposition have the same width $w_A = w_D = w$ and height unity. From Eq. (4.6) we obtain:

$$\begin{aligned} \alpha &= 1 - \cos\left(\tfrac{\pi}{2}\, w_A\right), \\ \beta &= \cos\left(\tfrac{\pi}{2}\,(1 - w_D)\right). \end{aligned} \tag{4.7}$$

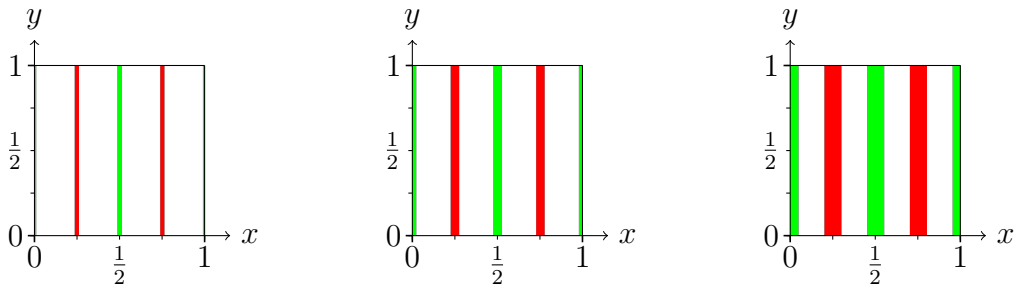

(a) $w = 0.05$ (b) $w = 0.1$ (c) $w = 0.2$

Figure 4.6: Vertical stripes (in the first half period) marking the regions of activation (green) defined by high shear ($s > 1 - \alpha$) and deposition (red) defined by low shear ($s < \beta$). The parameters α and β are calculated from the desired width $w_A = w_D = w$ (Eq. (4.7)).

In numerical simulations we systematically check the effects of the spatial extension of the activation and deposition regions on the productivity of reactions by changing the width w in steps of 0.02 from 0.02 to 0.2. In Fig. 4.6 the regions of activation and deposition are depicted for one half of a period. In the other half of a period the stripes are horizontal because of the horizontal direction of the shear.

(ii) In this case the regions of activation and deposition represent equal ranges in terms of shear ($\alpha = \beta$). The shear threshold parameter α is changed in steps

of 0.02 from 0.02 to 0.2. In Fig. 4.7 the activation and deposition regions are visualized for the first half of a period.

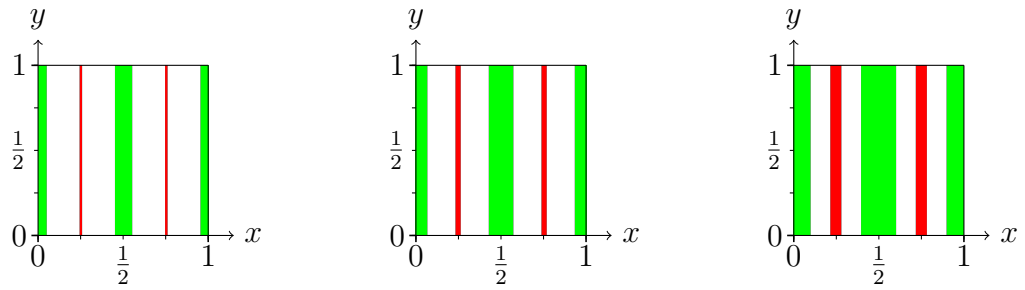

(a) $\alpha = 0.05$ (b) $\alpha = 0.1$ (c) $\alpha = 0.2$

Figure 4.7: Vertical stripes (in the first half period) marking the regions of activation (green) defined by high shear ($s > 1 - \alpha$) and deposition (red) defined by low shear ($s < \alpha$). The area of the stripes depends on the shear threshold parameter α as $w_A = 4 \cdot \frac{\arccos(1-\alpha)}{2\pi}$, $w_D = 1 - 4 \cdot \frac{\arccos(\alpha)}{2\pi}$.

The inflow region is modeled as a stripe of length unity and of height 0.1, from $y = 0$ to $y = 0.1$. The outflow region is modeled as a square of area 0.1, and is centered at $(0.25, 0.75)$. Figure 4.8 visualizes the inflow and outflow regions. Both regions must have the same area due to the incompressibility of the flow, each fluid element that is leaving the system must be replaced by a new fluid element entering the system.

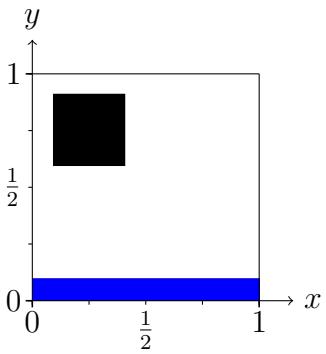

Figure 4.8: Regions of inflow (blue) and outflow (black) on the unit square. The inflow region is a stripe from $y = 0$ to $y = 0.1$ and the outflow region is a square of area 0.1, centered at $(0.25, 0.75)$.

5 Platelet activation at the vessel wall

This chapter is devoted to the study of the thrombus formation model defined in Section 4.4.1. Its main assumption is that platelets are activated and deposited in fixed spatial regions that are constant in time. First, we present the spatial distributions shown by the different types of platelets in this model. Next, we compute the deposited material both in numerical simulations and in a mean-field approach. Finally, we quantify the chaoticity of the dynamics and relate it to the fraction of deposited material.

5.1 Qualitative description of platelet dynamics: platelet distribution

We consider that the platelets are advected by the flow field given by Eqs. (4.1), and that resetting events, i.e., changes in the type of platelets, occur in the resetting regions (inflow, activation and deposition regions) shown in Fig. 4.5.

In this model, the spatial distribution of the platelets at a given time instance t is determined by the history of the system. The current state of a fluid element (i.e., the type of platelets it contains) is determined by the sequence of resetting regions it has visited at earlier times:

- The type of a platelet is passive, if the region it visited last time was the inflow region.
- The type of a platelet is deposited, if it visited the deposition region *and* it has visited the activation region at an earlier time.
- The type of a platelet is active, if it only visited the activation region during its history since it entered through the inflow region.

The most convenient way to obtain the asymptotic spatial distribution of the platelets is to start a trajectory from each spatial point and follow it backwards in time until it enters the inflow region. Then, according to the rules detailed above, a type can be associated to each spatial point depending on the regions visited by the trajectory under consideration.

In numerical simulations we define a 1000×1000 Cartesian lattice in the unit square, and follow trajectories starting from each lattice point backwards in time until they reach the inflow region. After each full period T of the flow we check the positions of the trajectories, and make changes in their types according to the above mentioned rules when they are found in one of the resetting regions. Between these discrete events at integer multiples of T, the types of the platelets are conserved. We investigate two particular cases, that of a deterministic flow with amplitude $a = 0.6$ and fixed phase $\varphi = 0$, and that of a flow with the same amplitude $a = 0.6$ and random phase φ.

In both cases we find that the three different types of platelets[1] are distributed in interwoven elongated filaments that have a Cantor set like fractal structure transverse to the filaments (see Fig. 5.1). This shows that the interplay between the chaotic hydrodynamics and biology maintains an imperfectly mixed stationary state.

The boundary of the filaments also has a complex fractal structure. Indeed, the boundary between the regions occupied by different platelets is the boundary between the basins of attraction of the resetting regions for the time-reversed advection dynamics. The structure of boundaries between basins of attraction of different attractors is a well-known problem in the field of chaotic dynamical systems [21, 30, 32]. The complicated fractal structure of the basin boundaries appears as a consequence of the chaotic saddle associated with the phenomena of transient chaos, i.e., with open flows.

Such boundaries are typical to open flows. Their appearance can be understood in a simple intuitive way. The resetting dynamics is equivalent to some kind of "biological opening" of the flow. More exactly, regarding the dynamics of the active platelets the activation region provides an inflow of active platelets, while the deposition region acts as an outflow region for these platelets. Similarly, the deposition region produces deposited platelets in the mixing region, thus it acts as an inflow of deposited platelets. The region where the empty spaces are filled again with pas-

[1] We recall that in our terminology the spatial distribution of deposited platelets refers to "empty" fluid elements from which the platelets have already been deposited.

sive platelets (i.e., the original inflow region of the model) acts as an outflow for deposited platelets. Finally, the passive platelets enter the mixing region through the inflow region, and leave it through the activation region. In conclusion, we have three different "biologically open" flows of the three types of platelets, with three different chaotic saddles governing their dynamics. The patterns shown in Fig. 5.1 visualize the unstable manifolds of the three chaotic saddles.

Since the size of the outflow regions (represented by the resetting regions in our model) is known to have strong influence on the characteristics of the unstable manifold [28], we run systematic simulations for different widths of the resetting regions. As a reference to the reader, the obtained patterns are presented in Appendix A.

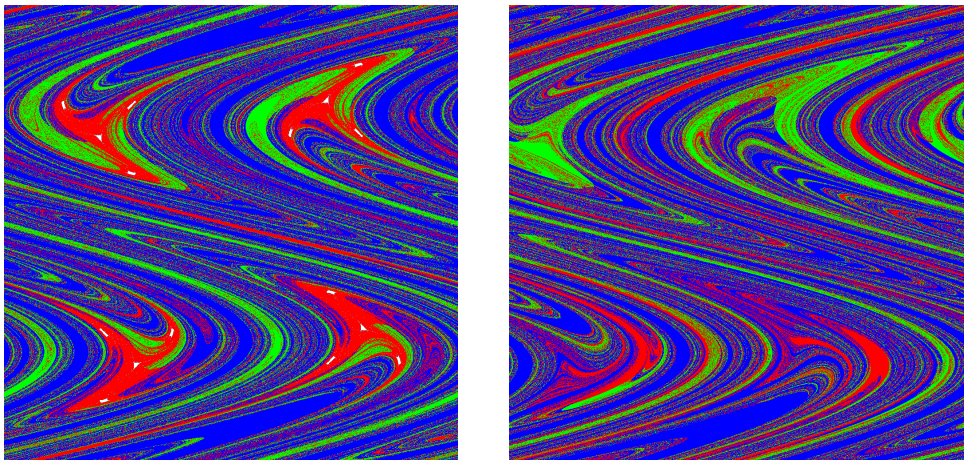

(a) $a = 0.6$, $\varphi = 0$ (b) $a = 0.6$ with random phase φ

Figure 5.1: Patterns of passive (blue), active (green), deposited (red) platelets for $w = w_I = 0.1$.

In the following, we characterize their fractal structure and relate it to the chaotic properties of the flow.

5.2 Quantitative description of the platelet dynamics

In this section we quantitatively characterize the parameter dependence of the platelet dynamics and compare it to analytical results obtained from a mean-field approximation. From the point of view of thrombus formation, the most relevant quantity is the amount of deposited platelets.

5.2.1 Mean-field approximation

In contrast to laminar flows, chaotic advection produces very efficient mixing in the system. Assuming the limit of perfect mixing, we can adopt a mean-field approach in which the adequate description of the dynamics is in terms of master equations.

We focus on the probabilities $P_X(t)$ that a fluid element carries a platelet of type X at time t, where $X \in \{A, P, D\}$ denotes the type of the different platelets: active, passive, and deposited, respectively. The probabilities $P_X(t)$ represent the relative number of the different types of platelets in the system at time t. To establish the master equations we have to identify first the possible transitions between the different states, as well as the transition rates of these processes. A schematical overview of the processes encountered in the model is presented in Fig. 5.2.

To establish the transition rates, we have to observe that the rates of the resetting processes are proportional to the area fraction of the phase space where resetting events can occur. For instance, passive platelets, distributed uniformly in the unit square, can change their type into active only in the activation region that has an area of $w_A \cdot 1 = w$. Thus, the transition rate from the passive to the active state is given by w. Similarly, active platelets can be deposited in the deposition region, giving the transition rate $w_D \cdot 1 = w$ from the active to the deposited state. Finally, both active and deposited platelets leaving through the outflow region are replaced by fresh passive platelets in the inflow region representing an area fraction of $w_I \cdot 1 = w_I = w_O$. Thus, both the transitions from active to passive, and from deposited to passive states are encountered with a rate w_O.

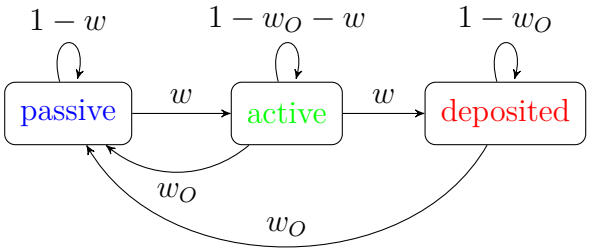

Figure 5.2: Schematic representation of the states of the system with the possible transitions and transition rates marked on the arrows.

With these transition rates the master equations can be written as:

$$\begin{aligned} \dot{P}_P &= w_O P_D + w_O P_A - w P_P, \\ \dot{P}_A &= w P_P - (w + w_O) P_A, \\ \dot{P}_D &= w P_A - w_O P_D. \end{aligned} \tag{5.1}$$

The relative number of different platelets in the asymptotic states can be obtained from Eqs. (5.1) by imposing the steady state condition

$$\dot{P}_X = 0 \qquad \text{for} \qquad X \in \{A, P, D\}$$

Using the normalization $P_P + P_A + P_D = 1$ and the notation $f \equiv w_O/w$ the steady state solutions can be obtained as

$$\begin{aligned} P_P^* &= f/(1+f)\,, \\ P_A^* &= f/(1+f)^2\,, \\ P_D^* &= 1/(1+f)^2\,. \end{aligned} \tag{5.2}$$

5.2.2 The fraction of deposited platelets in numerical simulations

In the following we compare the relative number of the different platelets obtained from numerical simulations to the solutions given by Eqs. (5.2). We measure the number of different platelets in the two-dimensional patterns shown in Fig. 5.1 and Appendix A, and divide them by the total number of platelets. The obtained values are shown in Fig. 5.3 for an inflow region of width $w_I = 0.1$ and different sizes w of the activation and deposition regions.

As expected, the relative number of passive platelets decreases as the width of the activation and deposition regions is increased. The number of active and passive platelets show a different tendency: as the activation and deposition regions grow, their number increases as well. At a certain point, the number of active platelets reaches a maximum, after which it starts decreasing with the growing width of the deposition region. From Eqs. (5.2) results that the maximum corresponds to $f = 1$, i.e., $w = w_I$. The number of deposited platelets show a monotone growth for increasing values of the width w of the deposition region.

Even though the mixing produced by chaotic advection is very efficient, it is still imperfect for $a \lesssim 0.8$ due to the the non-uniform, filamental structures present

in the phase space. Therefore, mean-field treatments of chaotic systems can lead to gross errors in some cases. Usually only systematic numerical simulations can decide whether a mean-field approximation can adequately describe the dynamics of a chaotic system.

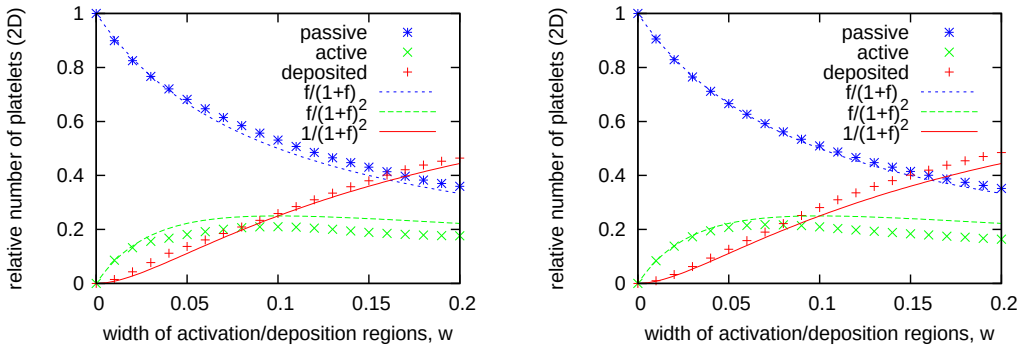

(a) $a = 0.6$, $\varphi = 0$ (b) $a = 0.6$ with random phase φ

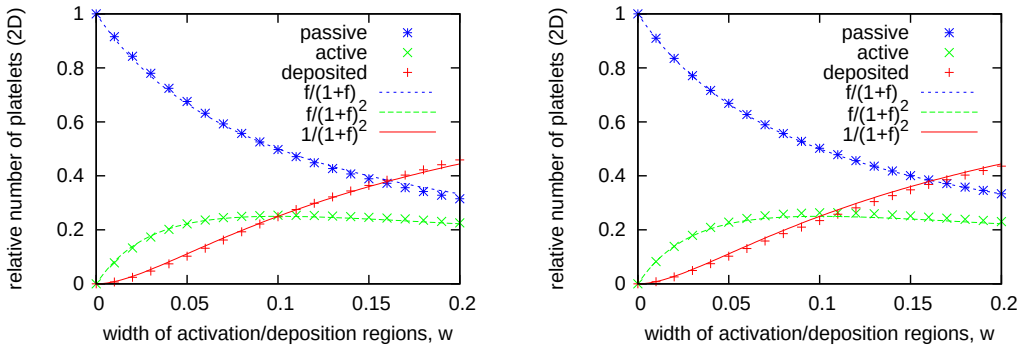

(c) $a = 0.8$, $\varphi = 0$ (d) $a = 1.4$, $\varphi = 0$

Figure 5.3: Relative number of platelets n_D vs. width of activation/deposition regions w for several amplitude and phase parameters. The width of the inflow region is $w_I = 0.1$. The relative number of platelets amount to the area fractions of the respective colors. The lines show the mean-field prediction from Eq. (5.2).

A more interesting issue is the role of the different degrees of imperfect mixing. The steady state solutions given by Eqs. (5.2) are valid in a perfectly mixed environment. The spatial patterns of the platelets presented in Fig. 5.1 and Appendix A, however, always show some degree of imperfect mixing. This can cause deviations from the solutions of the master equations.

We recall that the chaotic behavior of the flow is controlled by the amplitude a, in the sense that flows with higher values of the amplitude are more chaotic and produce

better mixing. In simulations, we compare cases with amplitudes $a = 0.6$, $a = 0.8$, and $a = 1.4$ (see the different panels of Fig. 5.3). From the lower panels of the figure it is clear that the master equations provide a fair description of the dynamics for high values of the amplitude: the amount of deposited and active platelets follow the steady state solutions given by Eqs. (5.2). For smaller amplitudes a, however, there is a systematic enhancement in the number of deposited platelets as compared to the expected values in well-mixed environment. We can attribute these deviations from the solutions Eqs. (5.2) to the chaoticity of the flow that produces irregular spatial patterns of platelets. The irregular patterns influence the biological dynamics.

The deviations from the solutions of the master equations caused by the chaotic flow are usually small: with few exceptions they are less than 10% of the expected values. Thus, the main role of the chaotic flow is to mix the platelets assuring that they visit the different resetting regions. The imperfect mixing, i.e., irregular spatial distribution of the platelets, seems to introduce only minor quantitative changes into the dynamics.

5.3 Characterization of chaotic properties: fractal dimensions

To shed more light on the interplay between the chaotic hydrodynamics and the biological dynamics, in the following we quantify the chaotic properties of the flow as well. The chaotic advection dynamics is governed by the chaotic saddle present in the mixing region. More exactly, in our model there are three different chaotic saddles that govern the dynamics of the three different types of platelets. The chaotic saddles have a fractal structure that can be characterized by the fractal dimension.

5.3.1 Mean-field approximation

In a mean-field approximation, we can calculate a theoretical estimate for the fractal dimensions of the different chaotic saddles. For this, we use the Kantz-Grassberger relation

$$D \approx 1 - \kappa/\bar{\lambda}, \tag{5.3}$$

that relates the fractal dimensions D of the chaotic saddles to the escape rates κ via the average Lyapunov exponents $\bar{\lambda}$.

Assuming a well-mixed environment, the escape processes can be considered proportional to the area of the region through which the platelets escape normalized by the area of the full chaotic region. The escape region for passive platelets is the activation region of area fraction w_A. Active platelets escape through the deposition and inflow region that represents an area fraction of $w_D + w_I$. Deposited platelets escape through the inflow region, i.e., in an area fraction of w_I. Thus the escape rates can be written as:

$$\begin{aligned} \kappa_P &= -\log(1 - w_A), \\ \kappa_A &= -\log(1 - w_I - w_D), \\ \kappa_D &= -\log(1 - w_I). \end{aligned} \tag{5.4}$$

The fractal dimensions corresponding to these values of the escape rates are shown in Fig. 5.4 with continuous lines.

5.3.2 Fractal dimensions measured in numerical simulations

The patterns shown in in Fig. 5.1 and Appendix A represent the unstable manifold of the chaotic saddle. Its fractal dimension D_{unst} is related to the fractal dimension of the chaotic saddle as $D_{unst} = 1 + D$. Thus, measuring the fractal dimension of the unstable manifold along a transect gives exactly the fractal dimension D of the chaotic saddle.

The spatial distribution of platelets along a line segment can be obtained with the method described in Section 5.1, i.e., by starting trajectories from the points of the line and iterating them backwards in time until they reach the inflow region. This allows us to reach high resolution easily for the one-dimensional transects without having to calculate the whole two-dimensional field.

We measure the fractal dimensions of the different types of platelets along a line segment situated at $y = 0.0$ by iterating 10^{20} time-reversed trajectories starting from this line. The simulations are run again for fixed values of the inflow region $w_I = 0.1$, and different widths w of the activation and deposition regions. The fractal dimensions are measured using the box-counting method. The results obtained for amplitude $a = 0.6$ of the flow (both for deterministic and randomized flows) are shown in Fig. 5.4.

In the limit $w = 0$ of the activation and deposition regions, the biological activity vanishes. In this case the "biological opening" of the flow is absent, thus the flow be-

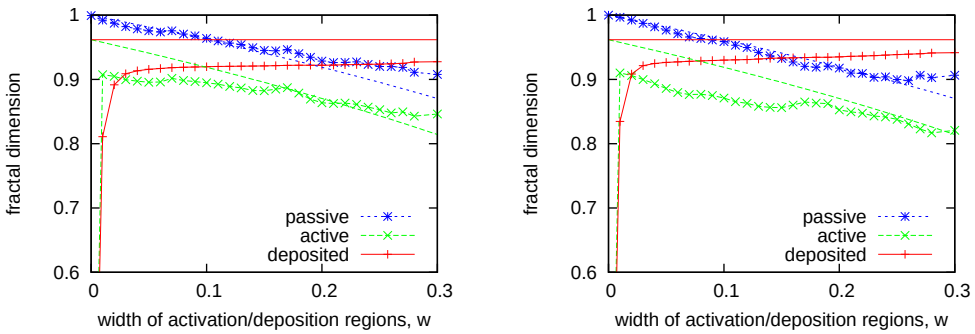

(a) $a = 0.6$, $\varphi = 0$ (b) $a = 0.6$ with random phase

Figure 5.4: Fractal dimensions of the passive (blue), active (green) and deposited (red) platelets as a function of the width w of the activation and deposition regions. The inflow region has a fixed width $w_I = 0.1$. The continuous lines are obtained from Eq. (5.3) using the measured values of the Lyapunov exponents $\bar{\lambda} = 2.75$, and the theoretical estimates Eqs. (5.4).

haves as a closed flow, i.e., the unstable manifold is a space filling, two-dimensional object with $D_{unst} = 2$. As the biological activity is turned on (i.e., $w \neq 0$), the unstable manifold of the passive platelets becomes a fractal, and its fractal dimension D_{unst} decreases as the width of the activation region w increases. The fractal dimension of the active platelets shows a similar tendency: it decreases as the width w of the deposition region increases. The deposited platelets, more exactly the empty fluid elements from which the platelets have been deposited, show a different behavior: their fractal dimension increases as the width of the deposition region increases, and it seems to saturate for large values of w.

The fractal dimensions measured in our numerical experiments show strong deviations from the mean-field expectation values. There are a number of reasons responsible for these deviations. First, (i) the orientation of the escape regions has a strong influence on the escape rates (for more details see Appendix B and reference [28]). While the activation and deposition stripes are narrow, this influence is strong. When the stripes become larger and cover a considerable part of the full mixing region, the role of the orientation decreases. Thus, this effect is responsible mainly for the deviations observed for small values of w. Further, (ii) the escape process is influenced by the actual number of platelets in the mixing region. When the width w of the activation and deposition regions is small, only few active and deposited platelets are present in the mixing region, thus a statistical description

is no longer valid for these types of platelets. And finally, (iii) the mean field description is valid only in the case when the mixing is strong enough to redistribute the platelets almost uniformly between two resetting events. For large values of w, however, this assumption fails, because the large activation and deposition regions produce large patches of active and deposited platelets that cannot be dispersed uniformly by the flow during one time period.

In conclusion, the mean-field approach provides only a rough approximant of the real escape rates and fractal dimensions of the chaotic saddles. For a proper characterization of the saddles, numerical simulations are needed that resolve the details of the fractal structures.

Nevertheless, the mean field approach has its own merits. It gives some theoretical insight into the behavior of the fractal dimensions as a function of the parameter w. It provides a better understanding of the logarithmic dependence of the fractal dimension of passive platelets on the width w of the activation region. It also explains the saturation observed on the dimension of the deposited platelets, and gives a theoretical estimate of the value at which this saturation occurs.

5.4 Interplay between the chaotic dynamics and biological dynamics

The deposition of platelets in the places where the blood flow exhibits chaotic behavior involves a complex interplay between the chaotic hydrodynamics and the biological dynamics of the platelets. The minimal chaotic advection model we investigated in this chapter clarified some steps of this interplay that can be outlined as follows:

(i) The chaotic advection assures a good mixing of the platelets in the region of interest that allows them to consecutively visit the activation and deposition regions. It also provides an inflow of fresh blood containing new passive platelets that replace the deposited ones.

(ii) The biological dynamics acts as a "biological opening" of the flow. This means that the activation and deposition regions select a chaotic saddle that will govern the dynamics. The size and geometry of the activation and deposition regions will determine the quantitative characteristics of the saddle. The existence of this saddle in the mixing region will cause a fractal spatial distribution

of the advected platelets. In the absence of the biological dynamics (see the case $w = 0$ in Fig. 5.4), the fractal structures do not appear in the dynamics, the distribution of the platelets is uniform, space-filling.

(iii) Subsequently, the irregular spatial distribution of platelets along a fractal has a feedback on the biological dynamics. This feedback will modify the amount of the deposited platelets and cause deviations from the mean-field expectation values. In general, there is no simple formula to estimate these deviations, since they depend on the detailed geometry of the fractal structures. The deviations gradually disappear as the chaoticity of the flow increases (for instance upon increasing the amplitude a) and provides a better mixing of the platelets.

To have a quantitative estimate of this latter effect, we compute the relative deviations

$$\Delta_D = \frac{n_d - n_{mean-field}}{n_{mean-field}}. \tag{5.5}$$

of the number of deposited platelets measured in simulations n_d from their mean-field expectation values $n_{mean-field}$ for the cases presented in Fig. 5.4a. Since we expect that the deviations Δ_D are caused by the fractal distribution of the active platelets, we plot these values as a function of the fractal dimension D_A of active platelets in Figure 5.5.

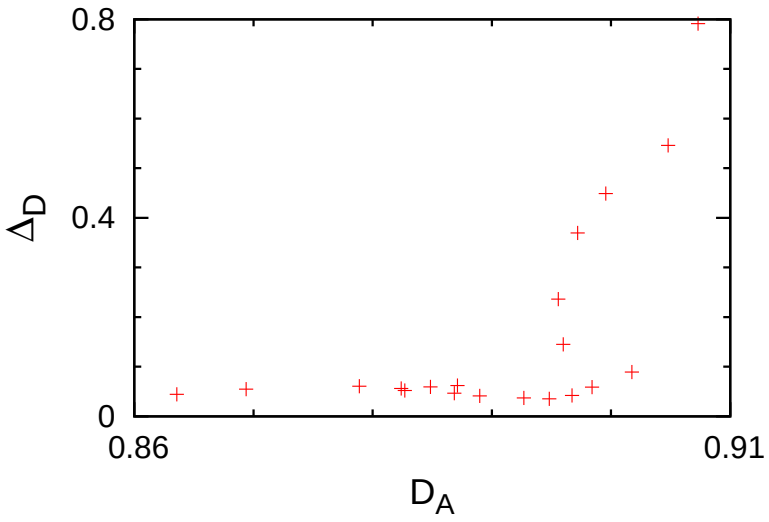

Figure 5.5: Relative deviations Δ_D of the deposited platelets from the mean-field expectation values as a function of the fractal dimension of active platelets.

As we can see, the deviations are rather small in the studied case, approximately $5-10\%$ of the mean field expectation value[2]. As already stated in the Section 5.2.2, the irregular spatial distribution of the platelets seems to introduce only minor quantitative changes into the dynamics.

[2]The higher values of $20-80\%$ represent cases where the mean field approximation is not valid because of the very small number (less than 14%) of deposited platelets in the mixing region.

6 Shear-induced platelet activation

In this chapter we investigate the thrombus formation model defined in Section 4.4.2, i.e., we consider the scenario in which platelets are activated by high shear of the flow and are deposited in regions of low shear. Since the blood flow is periodic in time, this results in activation and deposition regions that change in time according to the rhythm of the flow.

We follow the same steps as in the previous chapter: First we present a qualitative picture of the spatial distributions shown by the different types of platelets. Then we quantitatively characterize the biological and chaotic dynamics. Next, we compute the deposited material in numerical simulations and in a mean-field approach. Finally, we discuss the interplay between the hydrodynamics and biological dynamics.

As compared to the method of study used in the previous chapter, here we adopt a different approach. In the previous chapter we focused primarily on the steady-state *spatial distributions* of the platelets, and used the Kantz-Grassberger relation to obtain information about the *time evolution* of the system. Here in turn, we follow the *temporal evolution* of the system, and use the same formula to get insight into the *spatial distributions* of the platelets.

6.1 Qualitative description of platelet dynamics: platelet distribution

As in the previous chapter, we consider that the platelets are advected by the same flow field given by Eqs. 4.1, and that resetting events occur in discrete steps in the resetting regions. Here, however, the resetting regions (i.e., activation and deposition regions) are not localized in fixed spatial positions, but they always move to regions of the flow field that experience high and low shear-rates, respectively. Thus, they change their positions and orientations according to the time dependence of the flow. The positions of the activation and deposition regions in the first half of the

period are shown in Figs. 4.6 and 4.7. Apart from the positions of the activation and deposition regions, the biological dynamics follows the same rules as in the previous chapter.

We consider a sustained inflow of passive platelets: at each half period of the flow, a droplet of 10^5 passive platelets enters the mixing region through the inflow region shown in Fig. 4.8. The platelets spend some time in the mixing region, eventually participate in biological reactions and change their types, and finally they are washed out downstream. The outflow region, through which platelets can leave the mixing region, is also shown in Fig. 4.8.

We follow the trajectories of the platelets in the mixing region and keep evidence of the changes in their types. Fig. 6.1 shows a series of snapshots of the spatial distribution of platelets taken at different time instances.

We see that the first droplet of passive platelets gets elongated and folded by the chaotic flow. In places where the droplet encounters high shear rates, the platelets are activated. Then the continuous streching and folding by the flow produces a complex filamental distribution of the platelets that repeatedly crosses regions of high and low shear of the flow giving birth to new active and deposited platelets. Finally, in approximately 20 periods of the flow, the inflow and outflow balances each other and the spatial distribution of platelets approaches a *steady state*, in the sense that the filaments have time independent statistical properties, but they still move with the rhythm of the flow.

In conclusion, also in this case the chaotic flow maintains an imperfectly mixed stationary state in which the different types of platelets trace out *permanent* fractal structures: the unstable manifolds of the chaotic saddles.

Tuning the parameter a can change the chaoticity of the flow. Simulations run for higher values of the amplitude $|a| = 6.4$ exhibit the same kind of temporal evolution of the system: the repeated streching and folding produces the same complex filamental structure also in this case, but the overall appearance of the distribution is much closer to a well-mixed system. The other effect of the higher amplitude is that the remnants of the KAM tori visible in Fig. 6.1 are much smaller in this case.

As described in Section 4.4.2, we study two distinct cases where (i) $w_A = w_D = w$ and (ii) $\alpha = \beta$. In the second case the activation regions occupy a much larger area than the deposition regions. This results in a bigger amount of active platelets in the mixing region, that can be observed from a comparison of Fig. 6.1 and Fig. 6.2: in the latter the green color representing active platelets clearly dominates the picture.

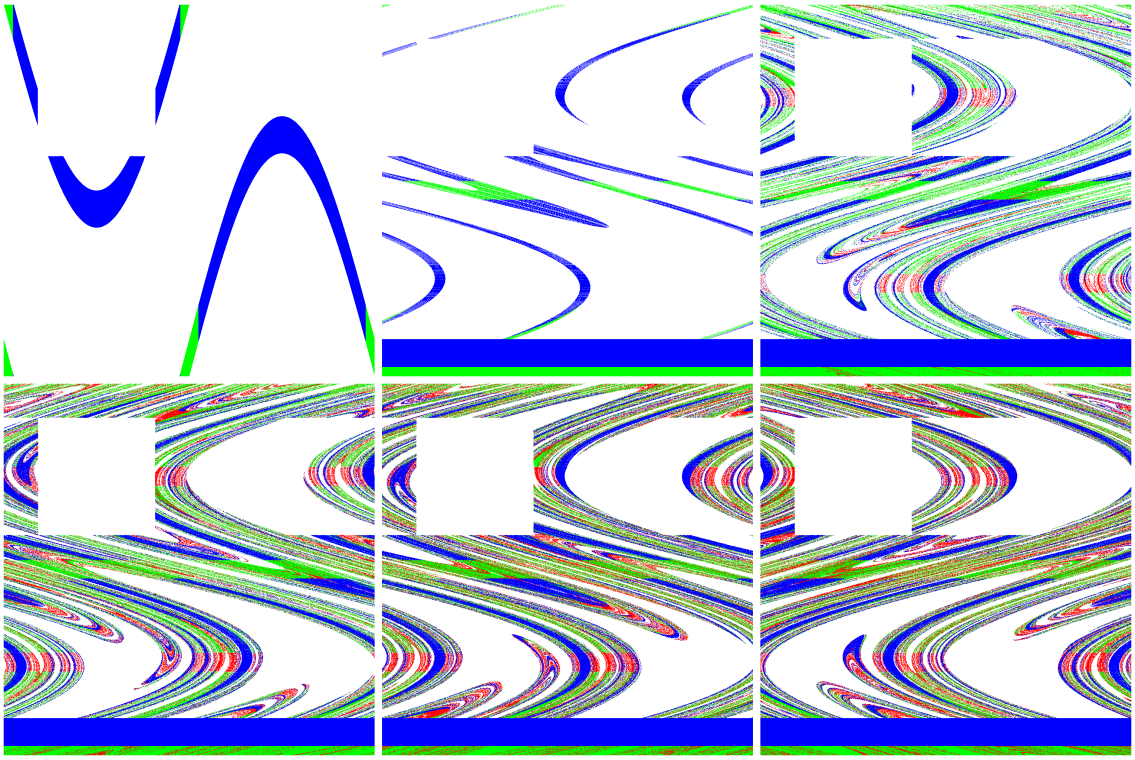

(a) $|a| = 0.6$

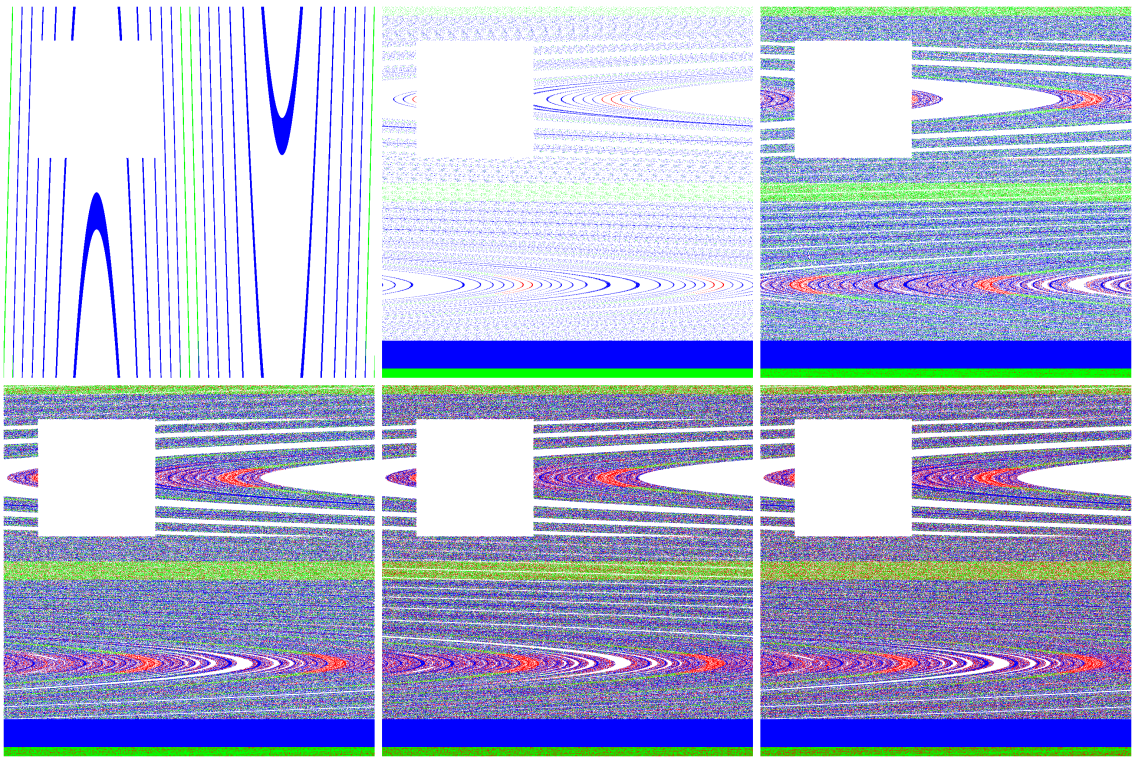

(b) $|a| = 6.4$

Figure 6.1: Patterns of the spatial distribution of passive (blue), active (green) and deposited (red) platelets for $w = 0.1$, $t/T = 0.5, 1, 5, 10, 15, 20$.

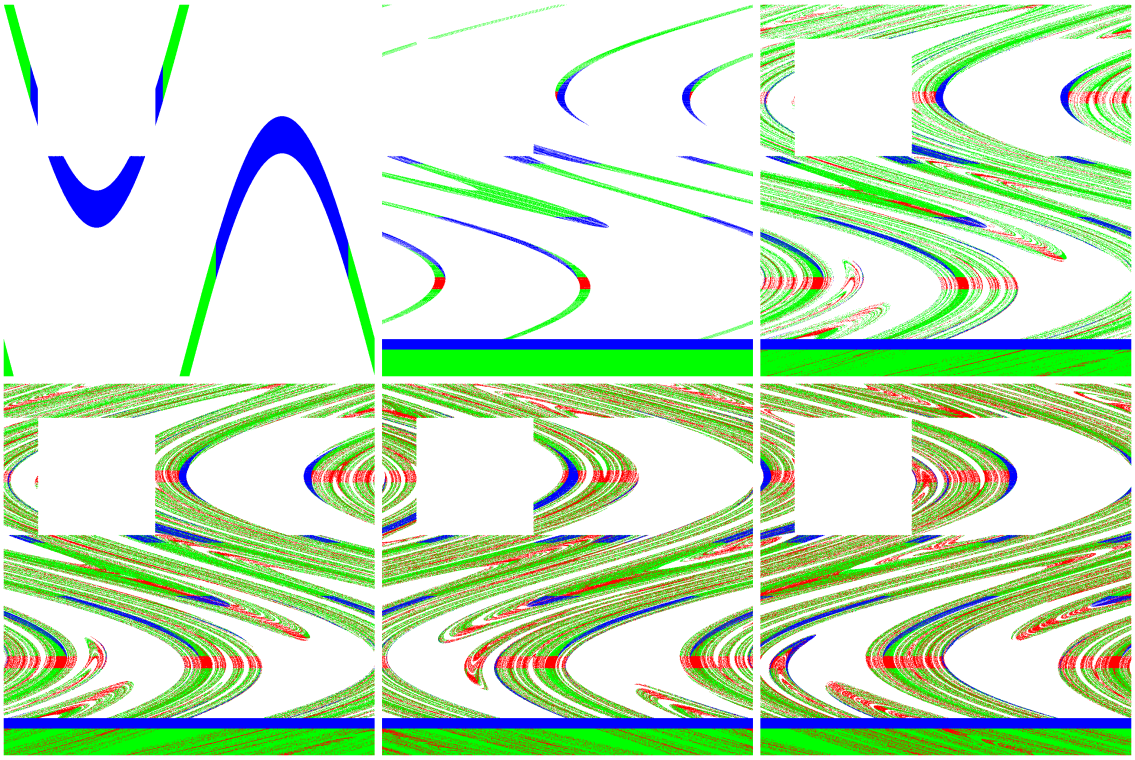

(a) $|a| = 0.6$

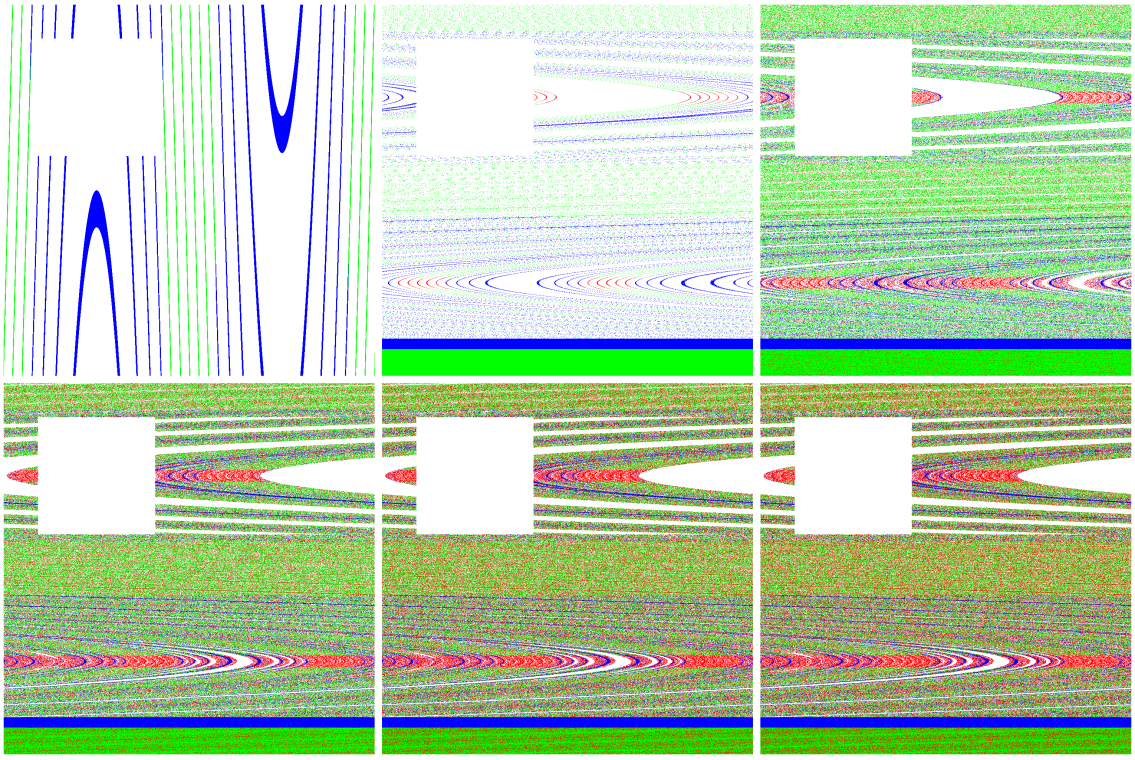

(b) $|a| = 6.4$

Figure 6.2: Patterns of the spatial distribution of passive (blue), active (green) and deposited (red) platelets for $\alpha = 0.1$, $t/T = 0.5, 1, 5, 10, 15, 20$.

6.2 Quantitative description of the platelet dynamics

We focus on the quantity of deposited platelets. We compute a mean-field expectation value and compare it to results obtained from numerical simulations.

6.2.1 Mean-field approximation

Assuming a well-mixed environment, we can establish master equations to describe the dynamics of the system. Compared to the case described in Section 5.2.1, there is an additional state of the platelets: those which left through the outflow region. The possible transitions between different states are represented in Fig. 6.3. The transition rates are given by the area fraction of the activation, deposition, and outflow regions, respectively.

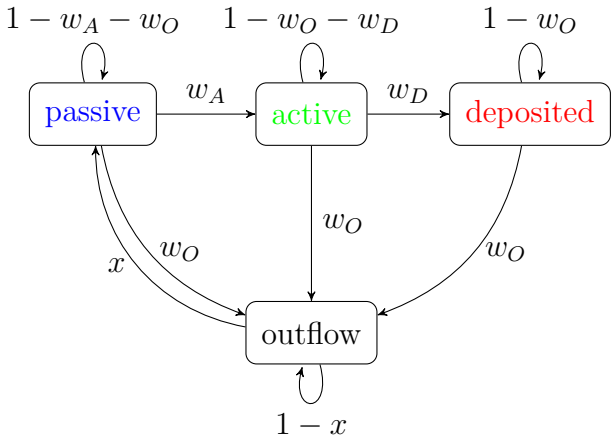

Figure 6.3: Schematic representation of the states of the system with the possible transitions and transition rates marked on the arrows. For one initial droplet $x = 0$, platelets leaving will not return. For the mean-field approximation we consider that the same amount of platelets or empty fluid elements that is leaving the system is returning as "fresh" passive platelets, thus $x = 1$.

The master equations can be written as:

$$\begin{aligned} \dot{P}_P &= w_O P_D + w_O P_A - w_A P_P, \\ \dot{P}_A &= w_A P_P - (w_D + w_O) P_A, \\ \dot{P}_D &= w_D P_A - w_O P_D. \end{aligned} \tag{6.1}$$

If we take into account that in an open flow platelets which escaped through the outflow region are immediately replaced by fresh blood containing passive platelets, in the scheme represented in Fig. 6.3 we can eliminate the outflow state and redirect all the incoming and outgoing transitions to the passive state. Thus, the scheme becomes topologically equivalent to the one presented in Section 5.2.1.

Using the notations $f_A \equiv w_O/w_A$ and $f_D \equiv w_O/w_D$ the steady state solutions of Eqs. (6.1) can be written as:

$$\begin{aligned} P_P^* &= f_A/(1+f_A)\,, \\ P_A^* &= f_D/(1+f_A)(1+f_D)\,, \\ P_D^* &= 1/(1+f_A)(1+f_D)\,. \end{aligned} \tag{6.2}$$

In the case $w_A = w_D = w$, these steady state solutions reduce to Eqs. (5.2) from Section 5.2.1.

6.2.2 The fraction of deposited platelets in numerical simulations

To measure the amount of deposited material, in numerical simulations we started one single droplet containing 10^5 passive platelets at time $t = 0$ from the inflow region, and counted the deposition events at each half period of the flow. The time evolution of this quantity is plotted in Fig. 6.4.

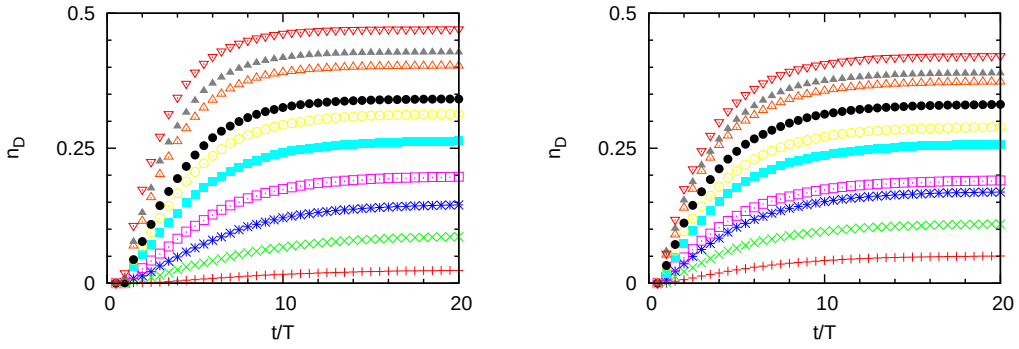

(a) same area in space (b) equal ranges in terms of shear

Figure 6.4: Fraction of deposited platelets n_D as a function of time. (a) Varying the widths of the stripes from $w = 0.02$ to $w = 0.2$ increasing in steps of 0.02. (b) Different values of the shear threshold α from 0.02 to 0.2 in steps of 0.02. In both cases the amplitude of the flow is $|a| = 0.6$.

After an initial increase, the number of deposited platelets saturates at a certain value. By this time the majority of the platelets from the original droplet got deposited or left the mixing region already, thus new deposition events do not occur unless fresh blood with passive platelets enters the mixing region.

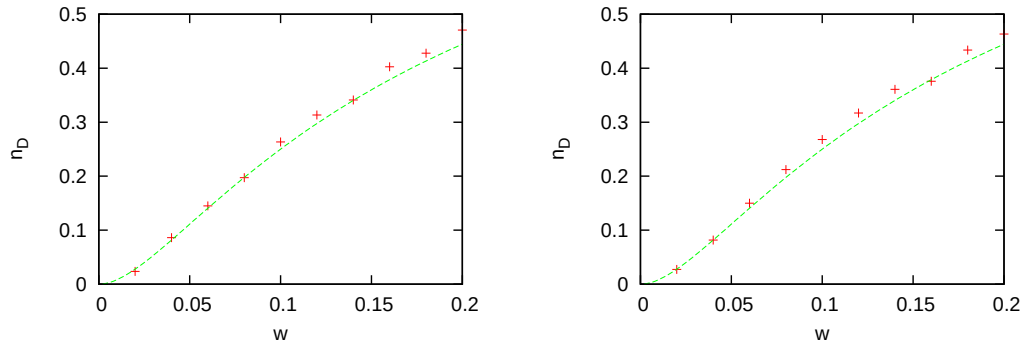

(a) $|a| = 0.6$ (b) $|a| = 6.4$

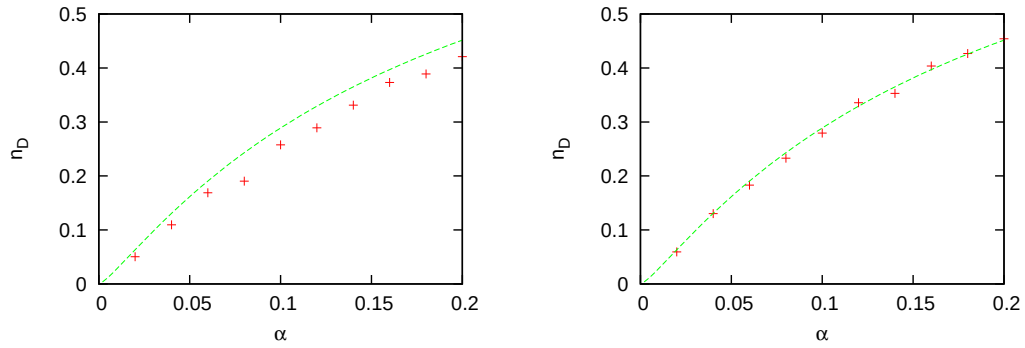

(c) $|a| = 0.6$ (d) $|a| = 6.4$

Figure 6.5: Fraction of deposited platelets at $t/T = 20$ vs. width w (top) and vs. α (bottom). The line shows the mean-field expectation from Eq. (6.2).

The total number of deposited platelets normalized by the total number of platelets from the initial droplet represents the fraction of deposited platelets in the steady state distribution in the case of a continuous inflow of platelets. Plotting this quantity along with the steady state solutions given by Eqs. (6.2) in Fig. 6.5 shows that the master equations give a fair description of the dynamics. There are small deviations from the mean-field expectation values that are due to the irregular spatial distribution of platelets.

6.3 Characterization of chaotic properties: escape rates

The chaotic dynamics observed in the mixing region of open chaotic flows is due to the presence of a chaotic saddle in the mixing region. In our model the situation is more complex, since there are different types of openings in the system. One is due to the outflow of particles that is associated with a chaotic saddle. The other is the "biological opening" of the flow discussed in the previous chapter, meaning that the transformation of passive platelets to active ones can be considered as an outflow of passive platelets. This causes an additional opening for the passive platelets and results in an additional saddle. Subsequently, the active platelets are changed to deposited platelets, which causes an additional opening for the active platelets' flow.

The escape of particles from the chaotic saddle is typically exponential [29] and can be characterized by the escape rate. The escape rate is determined by the structure of the saddle and it is uniquely related to the fractal dimension of the saddle via the Kantz-Grassberger relation (2.6).

Since in our case there are three different saddles, we expect that the escape rates (and the dimensions of the different saddles, respectively) are different for the different types of platelets.

We can calculate an estimate for the escape rates using a mean-field approximation analog to Section 5.2.1. Biological dynamics are happening twice each period in this model, thus the escape rates must be multiplied by a factor of 2. Because of the geometry of our model, the outflow region is covering a part of the deposition region of size $w_D \cdot \sqrt{w_O}$. This area needs to be substracted from the area fraction w_D. The resulting escape rates are:

$$\begin{aligned} \kappa_P &= -2\log(1-w_A), \\ \kappa_A &= -2\log(1-w_O-w_D+w_D\sqrt{w_O}), \\ \kappa_D &= -2\log(1-w_O). \end{aligned} \tag{6.3}$$

To obtain the escape rates numerically, we follow the time evolution of the number of active and deposited platelets in the mixing region. This number, indeed, exhibits an exponential decay (see Fig. 6.6 for different cases). The fact that active platelets escape not only through the outflow region, but also by deposition, is reflected by the faster decay of their number as compared to the decay of deposited platelets that can leave the mixing region only through the outflow region.

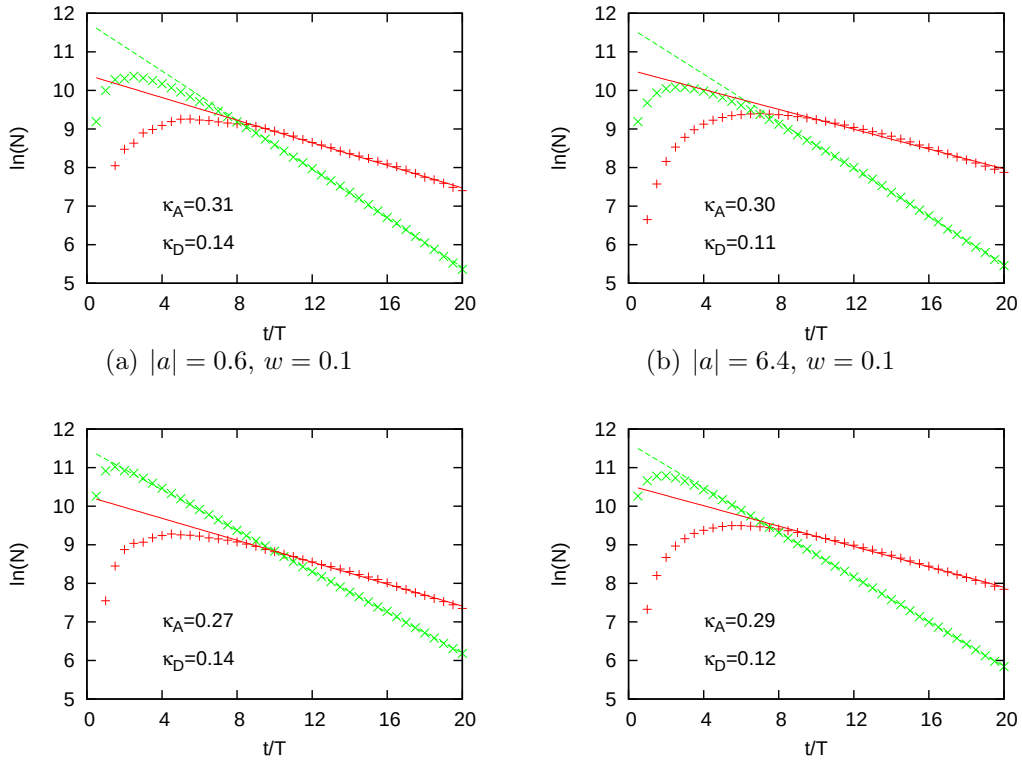

(a) $|a| = 0.6$, $w = 0.1$ (b) $|a| = 6.4$, $w = 0.1$

(c) $|a| = 0.6$, $\alpha = 0.1$ (d) $|a| = 6.4$, $\alpha = 0.1$

Figure 6.6: Exponential decay of the number N of active (green) and deposited (red) platelets.

To characterize the parameter dependence of the escape rates, we run systematic simulations (i) for various widths w of the resetting regions, and (ii) for various shear thresholds α defining the resetting regions. The results are summarized in Fig. 6.7. As expected, the escape rate of active platelets increases as the size of the deposition region increases, showing a logarithmical dependence $\kappa_A = -2\log(1 - w_O - w + w\sqrt{w_O})$ on the width w of this region.

The escape rate of deposited platelets shows in turn a surprising behavior. Since deposited platelets escape only through the outflow region that was kept constant in our simulations, we expect that the escape rate of the deposited platelets has a constant value $\kappa_D = -2\log(1 - w_O) = -2\log(0.9)$ over the whole range of widths w of the deposition region. In contrast to this naive expectation, the escape rate increases slightly with the width w in all studied cases.

The different escape rates of the different platelets demonstrate that their dynamics are governed by different chaotic saddles that can be characterized by different

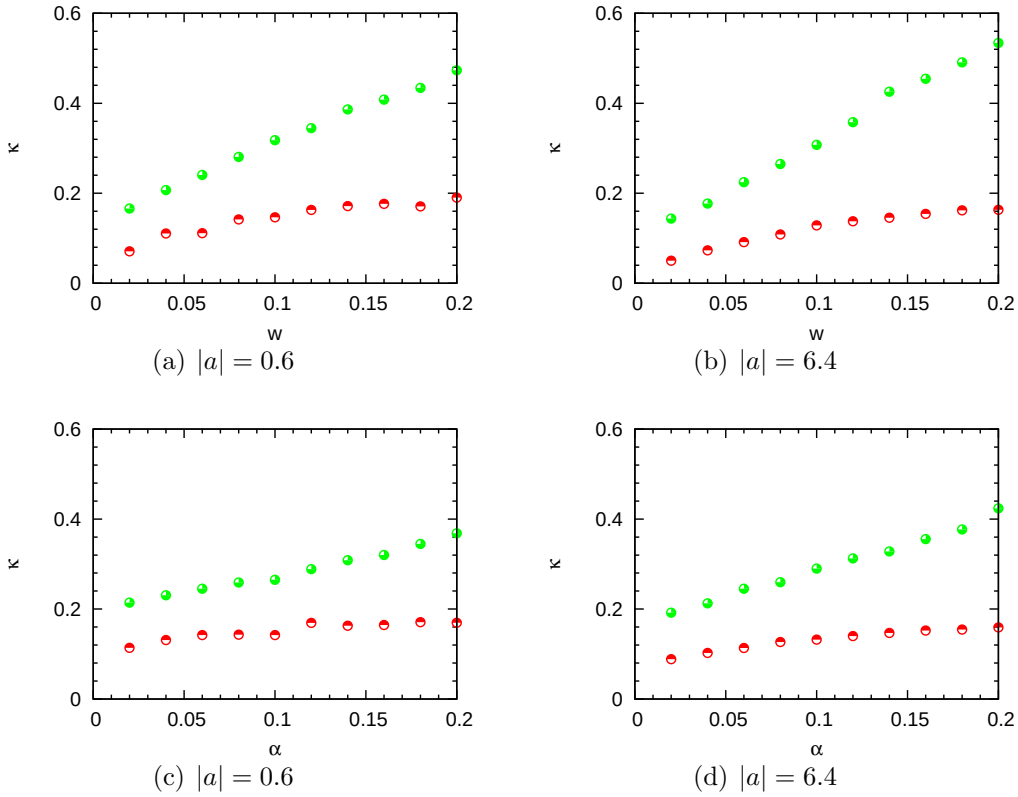

(a) $|a| = 0.6$ (b) $|a| = 6.4$

(c) $|a| = 0.6$ (d) $|a| = 6.4$

Figure 6.7: κ vs w, and κ vs α for active (green) and deposited (red) platelets.

fractal dimensions. One way to visualize and quantify the chaotic saddles is by using the box-counting method described in Chapter 3 and Appendix B. To apply this method, however, numerical simulations with high spatial resolution are necessary. A more convenient way to obtain the fractal dimension of the saddles is to compute them from the temporal behavior of the system, i.e., from the measured escape rates using the Kantz Grassberger relation (2.6) and the Lyapunov exponents $\lambda = 2.75$ and $\lambda = 12$ measured for the flow amplitudes $a = 0.6$ and $a = 6.4$, respectively.

6.4 Interplay between the chaotic dynamics and biological dynamics

Similarly to Section 5.4, the complex interplay between hydrodynamics and biological dynamics can be summarized in three main steps:

(i) The chaotic blood flow produces a good mixing of the platelets assuring that

they consecutively visit regions of high and low shear of the flow, thus they can be activated and deposited.

(ii) The biological dynamics selects a chaotic saddle and determines its quantitative characteristics. The activated and deposited platelets are distributed along the fractal filaments of the unstable manifold of the saddles. There is one remarkable difference, however, between the models discussed in Chapters 5 and 6. In the model used in the previous chapter the fractal structures appeared only as a consequence of the biological opening: the biology was the only mechanism to open the flow and make the chaotic saddles and other fractal structures visible. In the model treated in this chapter, a permanent fractality is present already in the advection dynamics, even in the absence of biological activity.

(iii) The fractal spatial distribution of the platelets has a feedback on the dynamics and causes deviations from the mean-field expectation values.

To compare the effects of the fractal distribution on the dynamics to those obtained in the previous chapter, we plot the deviations Δ_D defined by Eq. (5.5) as a function of the fractal dimension of the active platelets D_A in Fig. 6.8.

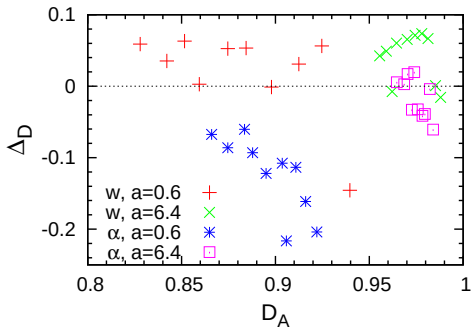

Figure 6.8: Relative deviation Δ_D of the fraction of deposited platelets from the mean-field expectation value as function of the fractal dimension of active platelets D_A.

The figure shows that the deviations are small also in this case. When the activation and deposition regions have equal spatial extents ($w_A = w_D = w$), the fraction of deposited platelets is higher than the mean-field expectation value regardless of the exact size of the resetting regions. When the width of the activation region is

much bigger than that of the deposition region, i.e., when both of them are determined by the same shear threshold α, the situation is changed and the measured values are in general below the mean-field expectation value. Finally, when the flow rate is increased (the case $|a| = 6.4$ corresponding to fractal dimensions close to 1), the deviations take both positive and negative values, showing that on average the mean-field approximation gives a fair description of the system.

7 Discussion and summary

In traditional studies of active processes taking place in blood, the possible effects of chaotic advection were usually disregarded. In the present work we addressed the problem of chaotic advection in the context of thrombus formation. We focused on sites where the vessel wall presented irregularities, either a constriction, or an enlargement, because these are the places where chaotic advection has been observed (see Figs. 4.1 and 4.2).

1. To describe the dynamics of platelets involved in thrombus formation, we constructed a minimal advection-reaction model. The advection dynamics was generated by a simple two-dimensional time-periodic flow that produced chaotic trajectories. The biological dynamics, i.e., the activation and subsequent deposition of platelets were represented by discrete resetting events. Resetting events took place only in well-defined spatial regions called activation and deposition regions.

2. We designed two idealized models:
   - In the first model the activation and deposition regions were localized and their position did not depend on the flow field. This model describes thrombus formation at the vessel wall, on sites where an injury occurs.
   - The second model considered platelet activation and deposition triggered by high and low shear rates of the flow. Consequently, the activation and deposition regions became time-dependent spatial regions that changed their locations according to the time dependence of the flow. This model is more adequate to describe atherosclerosis.

3. We adopted two different methods of study:
   - To obtain a high resolution of the spatial distributions, we identified the type of platelets by checking their history, i.e., by iterating trajectories

backward in time and following the resetting regions visited by the trajectory.

- To obtain more insights on the temporal evolution of the system we followed the trajectories forward in time.

Conclusion: The two methods gave similar quantitative results regarding the quantity of deposited material, thus they can be considered two equivalent and complementary approaches to study the phenomenon.

4. We quantified the productivity of reactions:
   - In a mean-field approach, we described the dynamics in terms of master equations. We found exact analytical solutions for the steady states of the system.
   - In numerical simulations we measured the quantity of deposited material and found that it is well-described by the solutions of the master equations.

   Conclusion: The deposited material can be expressed by Eqs. 5.2 and 6.2, and depends only on the area fraction of the different resetting regions.

5. We found permanent fractal structures in the spatial distributions of platelets. Conclusion: The interplay between the advection and biological dynamics involved in thrombus formation maintains an imperfect mixing.

6. We quantitatively characterized these fractal structures
   - by measuring fractal dimensions, and
   - by measuring escape rates.

   Conclusion: The naive mean-field expectation values do not show good agreement with the measured values. This is because these quantities depend on the detailed geometry of the spatial structures appearing in the phase space and there is no simple formula to calculate this dependence. Thus, the fractal dimensions and escape rates should be measured in direct numerical simulations.

7. We studied the interplay between chaotic hydrodynamics and biological dynamics, the conclusions are summarized in Sections 5.4 and 6.4.

The most surprising finding is that even though the interplay between the advection and biological dynamics involved in thrombus formation maintains an imperfect mixing of the platelets, the fractal structures that are clearly dominating the pictures in all the studied cases do not seem to have a significant effect on the productivity of the reactions: the deposited material is well described by the mean-field approach. However, before making a premature statement about the role of fractality, we should mention some factors that could diminish the effects of fractality:

- In our simulations, the resetting events take place in discrete steps at each half or full period of the flow. In such a long time, the flow can redistribute the advected platelets uniformly between two resettings, thus it washes out the effects of fractality. Choosing a smaller time step could reveal chaotic effects that are not observable in the simulations presented in the present work.

- A more elaborate model would take into account that only platelets which are in direct contact with activating agents are activated. This means that activation events can occur only on the surface of the fractal filaments, but not in the bulk where passive platelets do not have access to activators. This case is similar to acid-base reactions that are known to be drastically enhanced by the fractal distribution of the reagents.

- The final answer on the effects of fractality can be given by more realistic numerical simulations that explicitely take into account the flow fields presented in Figs 4.1. and 4.2.

A Unstable manifolds of the different types of platelets

The snapshots shown in Figs. A.1 and A.2 represent the unstable manifolds of the platelets for different widths w of the resetting regions as obtained from the model defined in Section 4.4.1.

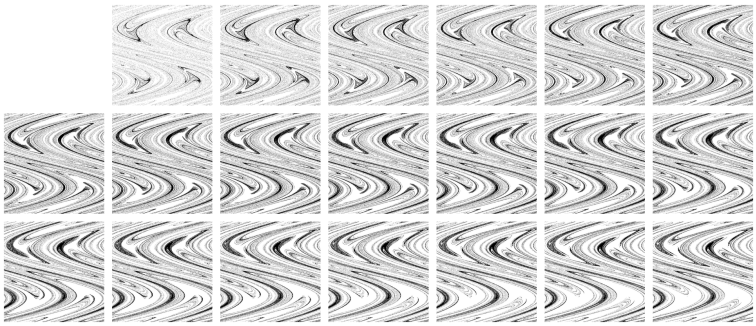

(a) active platelets

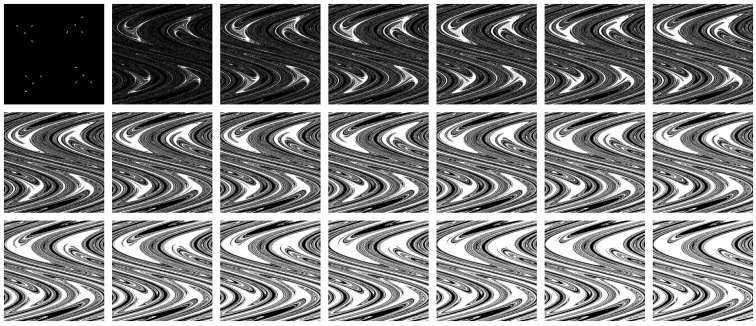

(b) passive platelets

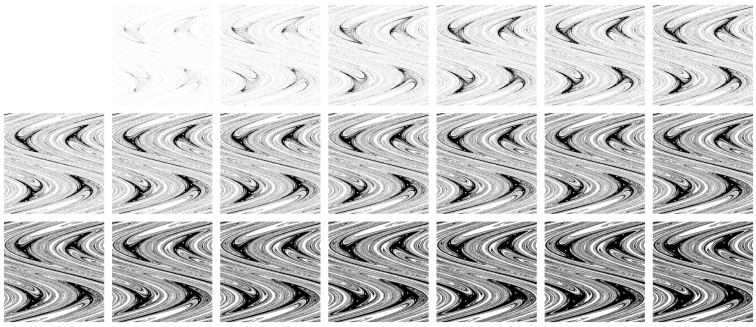

(c) deposited platelets

Figure A.1: The spatial distribution of the different types of platelets, calculated from Eq. (4.1) with fixed phase $\varphi = 0$. The width of the inflow region is fixed to $w_I = 0.1$, and the width of the two other regions is increased from $w = 0$ to $w = 0.2$ in steps of 0.01.

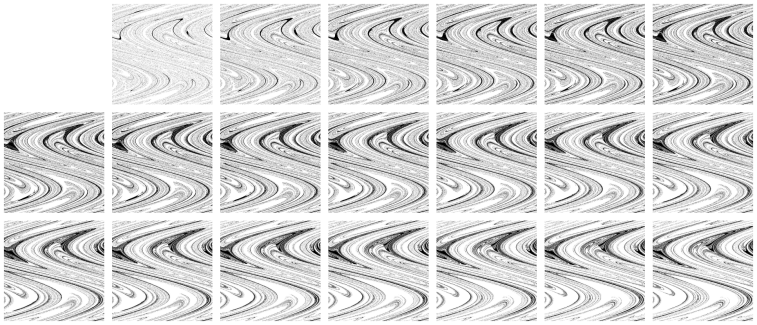

(a) active platelets

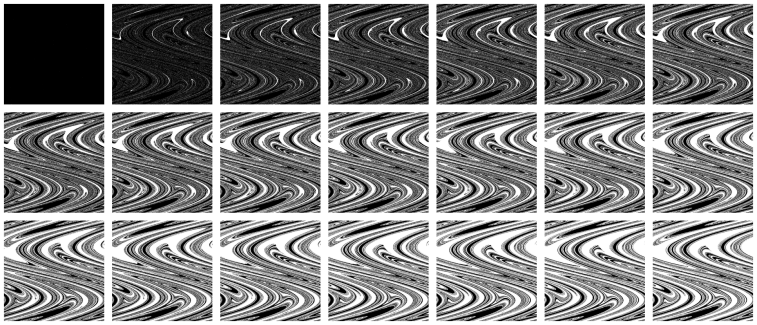

(b) passive platelets

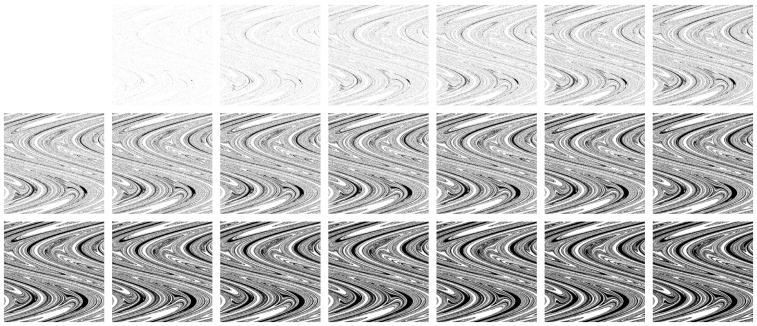

(c) deposited platelets

Figure A.2: A random phase is added to the argument of the sine map (Eq. (4.1)). All other parameters are chosen as described in Fig. A.1.

B Leaking dynamics

Chaotic advection has been typically treated separately for open (see for example [33] and references therein) and closed flows [19, 24]. The reason for this is that in the open case there is a well defined, permanent fractal characteristic due to the flux of fluid flowing through the system. This is the unstable manifold of the chaotic set as traced out by the advected particles. In contrast, in the closed case the unstable foliation is space-filling. A droplet placed in the closed flow will trace out a part of the unstable manifold for a while, but finally it will become uniformly distributed in the full two dimensional phase space (see Figure 2.2).

Under certain circumstances, however, the signatures of fractality become observable even in closed flows. The simplest way to visualize fractal structures in closed flows is to manually open the flow. Based on the findings of [28], we investigated effects of opening in the closed flow given by Eq.(4.1) with $a = 0.6, \varphi = 0$. We opened the flow by cutting a "leak" in the form of a stripe of width $w = 0.1$ and length unity, centered at $y = 0.5$, through which the particles can escape.

To **visualize the chaotic sets**, we followed 10^6 points – initially uniformly distributed in the unit square – for 20 periods. We removed all particles that entered the "leak". The positions of the non-escaped particles after 20 periods visualize the unstable manifold of the chaotic saddle, the positions 10 periods earlier show the saddle, and the initial positions of the particles represent the stable manifold (see Figure B.1). The stable and unstable manifolds are filamental structures, while the saddle has the typical Cantor set structure and, as expected, consists of the intersection points of the stable and unstable manifolds.

The "leaked" system, being an open flow, can be characterized by **escape rates**. To obtain the escape rate, we measured the time evolution of the number of particles in the mixing region and plotted the number of particles for each time T in a semi-logarithmic plot (Figure B.1). The slope of this plot gave the escape rate $\kappa = 0.09$.

Using the Kantz-Grassberger relation (2.6) and the numerically measured value $\lambda = 2.75$ of the Lyapunov exponent and $\kappa = 0.09$ of the escape rate, we can calculate

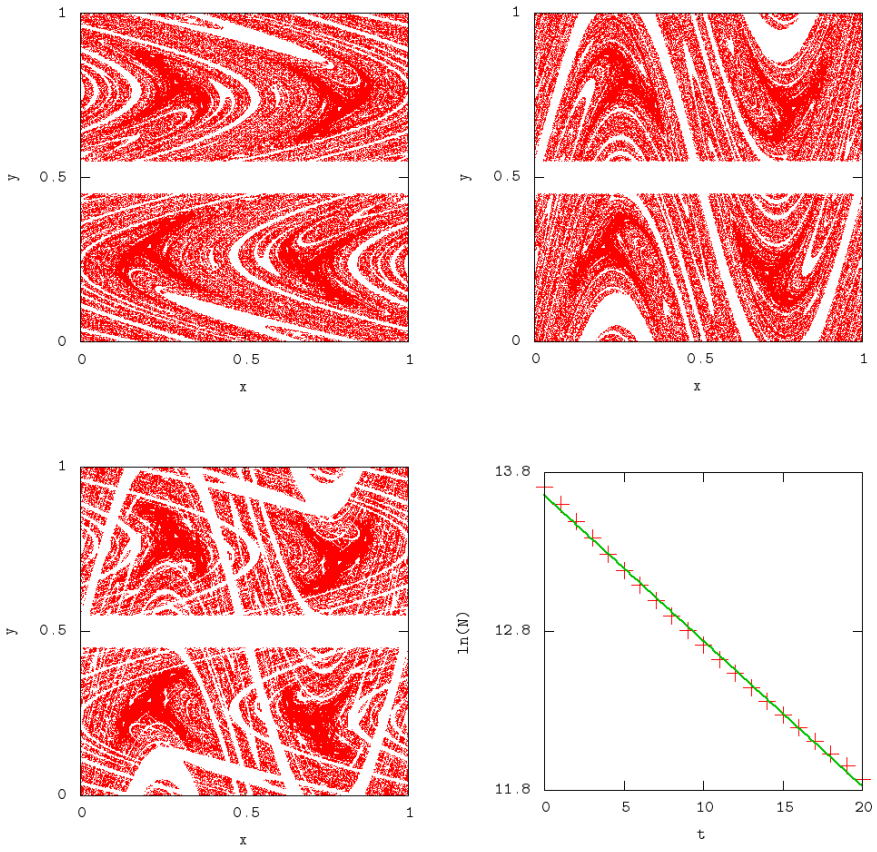

Figure B.1: Stable manifold (upper left) and unstable manifold (upper right), and saddle (lower left). In the lower right panel the plot used for the measurement of the escape rate is shown.

the fractal dimension of the chaotic saddle as $D = 0.967$. Using the same relation but the naive theoretical expectation for the escape rate $\kappa = -\ln(1 - w)$ we obtain $D = 0.961$, which is in good agreement with the numerically obtained value.

One important finding of [28] is that the escape rate strongly depends on the *orientation* of the leak. This is a surprising statement since in a closed flow where the unstable foliation is uniform and space filling, one might expect that the escape process depends on the area of the leaked region only. However, the unstable manifold that became visible by leaking the system has a strong spatial anisotropy. This anisotropy of the unstable foliation along which advected particles are accumulated results in the orientation dependence of the escape rates.

C Resetting dynamics

In order to maintain a nontrivial stationary distribution of tracers, earlier works (see for instance [19]) added source terms or sinks to the dynamics. A more realistic approach was suggested by Pierrehumbert [24], namely the resetting forcing. In this approach, tracers can be of two types and they change their types when they enter certain spatial domains of the flow (called resetting domains). The resetting dynamics was motivated by practical examples such as the thermal convection in a Rayleigh-Bernard cell, where the role of the resetting domains is played by the hot and cold plates. Another motivation is provided by the field of atmospheric sciences, that of chemical tracers in the stratosphere, where polar and equatorial regions play the role of the resetting zones.

In the numerical simulations we considered advection in the field of the alternating shear flow defined by Eqs. 4.1 and two resetting domains $\mathcal{D}_1$ and $\mathcal{D}_2$ of width $w = 2/15$ situated at the top and bottom of the unit square, centered at $y = 14/15$ and $y = 1/15$, respectively. The stationary tracer field was constructed from 1000x1000 uniformly distributed particles by calculating backwards trajectories until they reached one of the resetting regions (or a maximum of 100 iterations). Periodic boundaries were used in the x and y coordinate. We observed that the fractal structures became a permanent feature of the dynamics (Figure C.1, upper panels). The reason for this is that the resetting domain $\mathcal{D}_1$ acts as an inflow region for particles of type 1, domain $\mathcal{D}_2$ acts as outflow region, and thus the dynamics becomes formally open.

The residence time function was calculated on a line situated at $y = 0.5$ for 2000 points. The number of iterations needed to reach one of the resetting domains was measured for these points and plotted in Figure C.1. The irregularity of the residence time function is a typical feature of open chaotic advection because the time spent in the mixing region is very sensitive to the initial position. Particles on the stable manifold are trapped in the mixing region for long times and lead to singularities of the residence time. These infinitely many singularities are distributed on a fractal

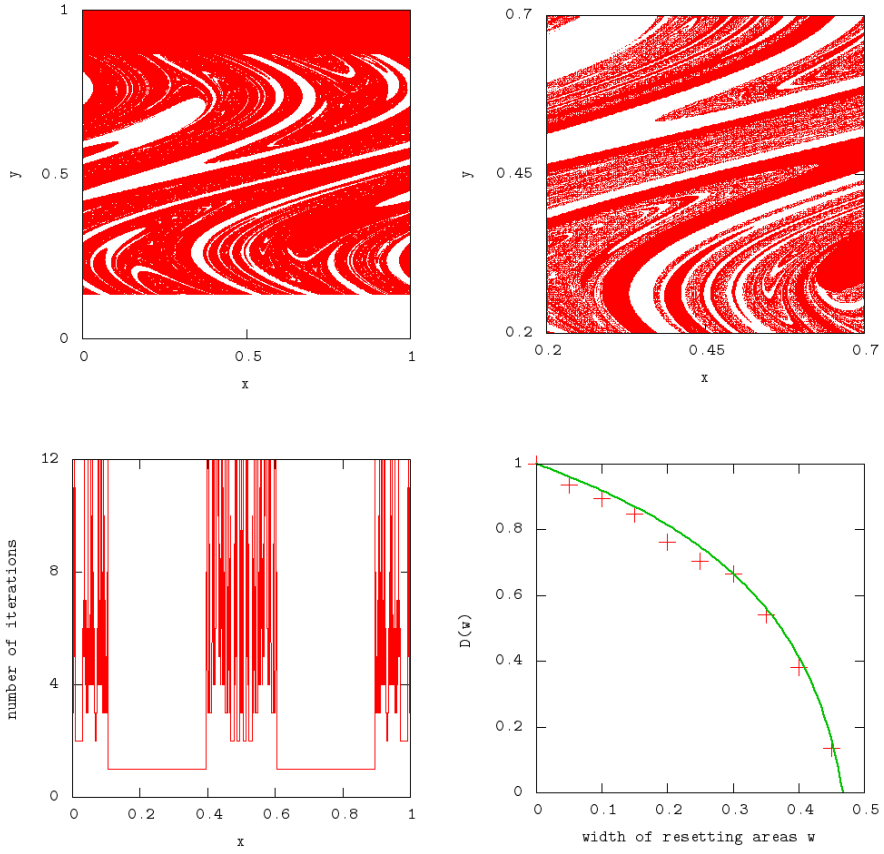

Figure C.1: Stationary fractal field (with magnification), residence time function (number of iterations), and fractal dimension for different sizes of the resetting domain.

set.

We also calculated the fractal dimension along a line situated at $y = 0.5$ using 2^{16} points along the line. We iterated the trajectories backwards in time until they reached one of the resetting zones. In these simulations, the centers of the resetting stripes were moved to 0.25 and 0.75, respectively. The fractal dimension was measured using the box-counting method described in the previous section. The measurements were repeated for different widths of the stripes. The numerically measured values of the fractal dimension are presented in Figure C.1 as red points along with a theoretical prediction based on the Kantz-Grassberger relation given by equation (2.6). In our case the escape rate κ in equation (2.6) was replaced by the resetting rate $\kappa = 1 - 2w$, and the Lyapunov exponent $\lambda = 2.75$ was measured

numerically.

Bibliography

[1] *Hyperbolicity and Sensitive Chaotic Dynamics at Homoclinic Bifurcations: Fractal Dimensions and Infinitely Many Attractors in Dynamics*. Cambridge University Press, 1995. ISBN 0521475724.

[2] The World Health Report. 2004. URL `http://www.who.int/entity/whr/2004/en/report04_en.pdf`.

[3] Hassan Aref. The development of chaotic advection. *Physics of Fluids*, 14(4): 1315–1325, 2002. doi: 10.1063/1.1458932.

[4] Siegfried Bleher, Edward Ott, and Celso Grebogi. Routes to chaotic scattering. *Phys. Rev. Lett.*, 63(9):919–922, Aug 1989. doi: 10.1103/PhysRevLett.63.919.

[5] Siegfried Bleher, Celso Grebogi, and Edward Ott. Bifurcation to chaotic scattering. *Phys. D*, 46(1):87–121, 1990. ISSN 0167-2789. doi: 10.1016/0167-2789(90)90114-5.

[6] Andrea Crisanti, Massimo Falcioni, Antonello Provenzale, Paolo Tanga, and Angelo Vulpiani. Dynamics of passively advected impurities in simple two-dimensional flow models. *Physics of Fluids A: Fluid Dynamics*, 4(8):1805–1820, 1992. doi: 10.1063/1.858402.

[7] Michael F. Doherty and Julio M. Ottino. Chaos in deterministic systems: Strange attractors, turbulence, and applications in chemical engineering. *Chemical Engineering Science*, 43(2):139 – 183, 1988. ISSN 0009-2509. doi: 10.1016/0009-2509(88)85029-2.

[8] F. Feudel, A. Witt, M. Gellert, J. Kurths, C. Grebogi, and M.A.F. Sanjuán. Intersections of stable and unstable manifolds: the skeleton of lagrangian chaos. *Chaos, Solitons & Fractals*, 24(4):947 – 956, 2005. ISSN 0960-0779. doi: 10.1016/j.chaos.2004.09.059.

[9] Christian Gachet. Regulation of platelet functions by p2 receptors. *Annual Review of Pharmacology and Toxicology*, 46(1):277–300, 2006. doi: 10.1146/annurev.pharmtox.46.120604.141207.

[10] Celso Grebogi, Edward Ott, and James A. Yorke. Crises, sudden changes in chaotic attractors, and transient chaos. *Physica D: Nonlinear Phenomena*, 7 (1-3):181 – 200, 1983. ISSN 0167-2789. doi: 10.1016/0167-2789(83)90126-4.

[11] Cornelia Hahn and Martin A. Schwartz. Mechanotransduction in vascular physiology and atherogenesis. *Nat Rev Mol Cell Biol*, 10(1):53–62, 2009. doi: 10.1038/nrm2596.

[12] Hermann Haken. *Synergetik*. Springer-Verlag, 3rd edition, 1990. ISBN 3540516921.

[13] Guan-Hsong Hsu, Edward Ott, and Celso Grebogi. Strange saddles and the dimensions of their invariant manifolds. *Physics Letters A*, 127(4):199 – 204, 1988. ISSN 0375-9601. doi: 10.1016/0375-9601(88)90102-8.

[14] Mark L. Kahn, Yao-Wu Zheng, Wei Huang, Violeta Bigornia, Dewan Zeng, Stephen Moff, Robert V. Farese, Carmen Tam, and Shaun R. Coughlin. A dual thrombin receptor system for platelet activation. *Nature*, 394(6694):690–694, August 1998. ISSN 0028-0836. doi: 10.1038/29325.

[15] H. Kantz and P. Grassberger. Repellers, semi-attractors, and long-lived chaotic transients. *Physica D: Nonlinear Phenomena*, 17(1):75 – 86, 1985. ISSN 0167-2789. doi: 10.1016/0167-2789(85)90135-6.

[16] M. H. Kroll, J. D. Hellums, L. V. McIntire, A. I. Schafer, and J. L. Moake. Platelets and shear stress. *Blood*, 88(5):1525–1541, 1996.

[17] Sarah Köster, Jennie B. Leach, Bernd Struth, Thomas Pfohl, and Joyce Y. Wong. Visualization of Flow-Aligned Type I Collagen Self-Assembly in Tunable pH Gradients. *Langmuir*, 23(2):357–359, January 2007. ISSN 0743-7463. doi: 10.1021/la062473a.

[18] Jeroen S. W. Lamb and John A. G. Roberts. Time-reversal symmetry in dynamical systems: A survey. *Physica D: Nonlinear Phenomena*, 112(1-2):1 – 39, 1998. ISSN 0167-2789. doi: 10.1016/S0167-2789(97)00199-1. Proceedings of the Workshop on Time-Reversal Symmetry in Dynamical Systems.

[19] Zoltán Neufeld, Cristóbal López, and Peter H. Haynes. Smooth-Filamental Transition of Active Tracer Fields Stirred by Chaotic Advection. *Physical Review Letters*, 82(12):2606–2609, 1999. doi: 10.1103/PhysRevLett.82.2606.

[20] Zoltán Neufeld, Peter H. Haynes, and Guillemette Picard. The effect of forcing on the spatial structure and spectra of chaotically advected passive scalars. *Physics of Fluids*, 12(10):2506–2513, 2000. doi: 10.1063/1.1289504.

[21] Edward Ott. *Chaos in Dynamical Systems*. Cambridge University Press, 2nd edition, 2002. ISBN 0521010845.

[22] Julio M. Ottino. *The Kinematics of Mixing*. Cambridge University Press, 1989. ISBN 0521368782.

[23] Áron Péntek, Zoltán Toroczkai, Tamás Tél, Celso Grebogi, and James A. Yorke. Fractal boundaries in open hydrodynamical flows: Signatures of chaotic saddles. *Phys. Rev. E*, 51(5):4076–4088, May 1995. doi: 10.1103/PhysRevE.51.4076.

[24] Raymond T. Pierrehumbert. Tracer microstructure in the large-eddy dominated regime. *Chaos, Solitons & Fractals*, 4(6):1091 – 1110, 1994. ISSN 0960-0779. doi: 10.1016/0960-0779(94)90139-2. Special Issue: Chaos Applied to Fluid Mixing.

[25] J. A. G. Roberts and G. R. W. Quispel. Chaos and time-reversal symmetry. order and chaos in reversible dynamical systems. *Physics Reports*, 216(2-3):63 – 177, 1992. ISSN 0370-1573. doi: 10.1016/0370-1573(92)90163-T.

[26] J. Evan Sadler. Biochemistry and genetics of von Willebrand factor. *Annual Review of Biochemistry*, 67(1):395–424, 1998. doi: 10.1146/annurev.biochem.67.1.395.

[27] A. B. Schelin, Gy. Károlyi, A. P. S. de Moura, N. A. Booth, and C. Grebogi. Chaotic advection in blood flow. *Phys. Rev. E*, 80(1):016213, Jul 2009. doi: 10.1103/PhysRevE.80.016213.

[28] Judit Schneider, Tamás Tél, and Zoltán Neufeld. Dynamics of “leaking" hamiltonian systems. *Phys. Rev. E*, 66(6):066218, Dec 2002. doi: 10.1103/PhysRevE.66.066218.

[29] Tamás Tél. Transient chaos. *Directions in Chaos*, 3, 1990. Edited by H. Bai-Lin (World Scientific, Singapore, 1991).

[30] Tamás Tél and Márton Gruiz. *Chaotic Dynamics*. Cambridge University Press, 2006. ISBN 0521547830.

[31] Tamás Tél, Takashi Nishikawa, Adilson E. Motter, Celso Grebogi, and Zoltán Toroczkai. Universality in active chaos. *Chaos: An Interdisciplinary Journal of Nonlinear Science*, 14(1):72–78, 2004. doi: 10.1063/1.1626391.

[32] Z. Toroczkai, G. Károlyi, Á. Péntek, T. Tél, C. Grebogi, and J. A. Yorke. Wada dye boundaries in open hydrodynamical flows. *Physica A Statistical Mechanics and its Applications*, 239:235–243, February 1997.

[33] Tamás Tél, Alessandro de Moura, Celso Grebogi, and György Károlyi. Chemical and biological activity in open flows: A dynamical system approach. *Physics Reports*, 413(2-3):91 – 196, 2005. ISSN 0370-1573. doi: 10.1016/j.physrep.2005.01.005.

[34] Lei Yu, Edward Ott, and Qi Chen. Transition to chaos for random dynamical systems. *Phys. Rev. Lett.*, 65(24):2935–2938, Dec 1990. doi: 10.1103/PhysRevLett.65.2935.

[35] E.M. Ziemniak, C. Jung, and T. Tél. Tracer dynamics in open hydrodynamical flows as chaotic scattering. *Physica D: Nonlinear Phenomena*, 76(1-3):123 – 146, 1994. ISSN 0167-2789. doi: 10.1016/0167-2789(94)90255-0.

Danksagung

Ich möchte an dieser Stelle allen danken, die zum Gelingen dieser Arbeit beigetragen haben. Dazu gehören die Mitarbeiter der Abteilung Dynamik komplexer Fluide, bei denen ich mich sehr wohl gefühlt habe und insbesondere die Arbeitsgruppe von Jürgen Vollmer, die immer für gute Laune und interessante Diskussionen gesorgt hat.

Besonderer Dank gilt Izabella Benczik für ihre umfangreiche Betreuung, die vielen Korrekturen, Erläuterungen und Diskussionen, ebenso Jürgen Vollmer, der zu jeder Tageszeit für Fragen und Diskussionen ansprechbar war. Ich danke auch György Károlyi und seinen Mitarbeitern für die Gastfreundschaft und die tolle Einführung in die Thematik, die meisten verwendeten Methoden habe ich von ihm gelernt. Eberhard Bodenschatz möchte ich für seine Beteiligung als Gutachter danken.

Nicht zuletzt möchte ich auch meiner Familie danken, die mir mein Studium finanziell und moralisch ermöglicht und immer Geduld zeigte, wenn ich von letzterem vollständig in Anspruch genommen wurde.

Erklärung nach §13(8)der Prüfungsordnung für den Bachelor-Studiengang Physik und den Master-Studiengang Physik an der Universität Göttingen:

Hiermit erkläre ich, dass ich diese Abschlussarbeit selbständig verfasst habe, keine anderen als die angegebenen Quellen und Hilfsmittel benutzt habe und alle Stellen, die wörtlich oder sinngemäß aus veröffentlichten Schriften entnommen wurden, als solche kenntlich gemacht habe.
Darüberhinaus erkläre ich, dass diese Abschlussarbeit nicht, auch nicht auszugsweise, im Rahmen einer nichtbestandenen Prüfung an dieser oder einer anderen Hochschule eingereicht wurde.

Göttingen, den 14. Juni 2010

(Mitja Kleider)